Received: 22 January 2017 | Revised: 26 May 2017 | Accepted: 23 June 2017

DOI: 10.1002/jmor.20728

RESEARCH ARTICLE

WILEY JOURNAL OF morphology

Interspecific variation in the tetradactyl manus of modern tapirs (Perissodactyla: *Tapirus*) exposed using geometric morphometrics

Jamie A. MacLaren[1] | Sandra Nauwelaerts[1,2]

[1]Department of Biology, Universiteit Antwerpen, Building D, Campus Drie Eiken, Universiteitsplein, Wilrijk, Antwerp 2610, Belgium

[2]Centre for Research and Conservation, Koninklijke Maatschappij voor Dierkunde (KMDA), Koningin Astridplein 26, Antwerp 2018, Belgium

Correspondence
Jamie A. MacLaren, Room D1.41, Building D, Campus Drie Eiken, Universiteitsplein 1, 2610 Antwerp, Belgium.
Email: jamie.maclaren@uantwerpen.be

Funding information
FWO (Fonds Wetenschappelijk Onderzoek) scholarship awarded to JM and BOF-UA (Special Research Fund for Universiteit Antwerpen) research grant awarded to SN.

Abstract

The distal forelimb (autopodium) of quadrupedal mammals is a key morphological unit involved in locomotion, body support, and interaction with the substrate. The manus of the tapir (Perissodactyla: *Tapirus*) is unique within modern perissodactyls, as it retains the plesiomorphic tetradactyl (four-toed) condition also exhibited by basal equids and rhinoceroses. Tapirs are known to exhibit anatomical mesaxonic symmetry in the manus, although interspecific differences and biomechanical mesaxony have yet to be rigorously tested. Here, we investigate variation in the manus morphology of four modern tapir species (*Tapirus indicus*, *Tapirus bairdii*, *Tapirus pinchaque*, and *Tapirus terrestris*) using a geometric morphometric approach. Autopodial bones were laser scanned to capture surface shape and morphology was quantified using 3D-landmark analysis. Landmarks were aligned using Generalised Procrustes Analysis, with discriminant function and partial least square analyses performed on aligned coordinate data to identify features that significantly separate tapir species. Overall, our results support the previously held hypothesis that *T. indicus* is morphologically separate from neotropical tapirs; however, previous conclusions regarding function from morphological differences are shown to require reassessment. We find evidence indicating that *T. bairdii* exhibits reduced reliance on the lateral fifth digit compared to other tapirs. Morphometric assessment of the metacarpophalangeal joint and the morphology of the distal facets of the lunate lend evidence toward high loading on the lateral digits of both the large *T. indicus* (large body mass) and the small, long limbed *T. pinchaque* (ground impact). Our results support other recent studies on *T. pinchaque*, suggesting subtle but important adaptations to a compliant but inclined habitat. In conclusion, we demonstrate further evidence that the modern tapir forelimb is a variable locomotor unit with a range of interspecific features tailored to habitual and biomechanical needs of each species.

KEYWORDS
discriminant function, locomotion, manus, mesaxonic symmetry, *Tapirus bairdii*

1 | INTRODUCTION

Modern tapirs (Tapiridae; *Tapirus* Brünnich) are enigmatic, forest-dwelling representatives of the order Perissodactyla (odd-toed ungulates) (Cozzuol et al., 2013; Ruiz-García et al., 2012; Steiner & Ryder, 2011). In addition to equids (horses, asses, and zebras) and rhinoceroses, tapirs represent the last members of a formerly highly speciose order of small to very large herbivores (Janis, 1989; Norman & Ashley, 2000). The tetradactyl (four-toed) manus of the modern tapir is a unique feature in extant perissodactyls, with equids and rhinoceroses having reduced their functional digit number to one and three, respectively (MacFadden, 1992); the earliest ancestors of rhinoceroses, tapirs, and equids also displayed a tetradacyl manus (Holbrook, 2001). The small, basal members of the Perissodactyla (e.g., *Propalaeotherium*, *Hyracotherium*, *Heptodon*) are interpreted as forest-dwelling browsers with a 'ancestral' digital condition, bearing three toes on the hind foot (tridactyly), and four on the forefoot (Hellmund, 2005; Holbrook, 2001; Radinsky, 1965; Wood et al., 2010). This plesiomorphic characteristic

of the tapir manus, among other features of tapir anatomy, has contributed to the traditional interpretation of tapirs as 'living fossils' (Hershkovitz, 1954; Janis, 1984; Padilla, Dowler, & Downer, 2010; Schoch, 1989). Consequently, extant tapirs have been the object of numerous morphological and ecological comparisons to extinct tetradactyl perissodactyls (including Holbrook, 2001, 2009; Janis, 1984; Radinsky, 1965). However, these studies often treat *Tapirus* either as a single morphological unit (e.g., Holbrook, 1999, 2001), or compare only one or two species of *Tapirus* with extinct tetradactyl perissodactyls (e.g., Radinsky, 1965; Simpson, 1945). Recent studies on the extinct tapirs of North America are beginning to increase species counts when performing comparative analyses, albeit with predominantly qualitative techniques (Holanda, Ribeiro, & Ferigolo, 2012; Hulbert, 1995, 2005, 2010; Hulbert et al., 2009). Using *Tapirus* as a solitary morphological unit is greatly beneficial for phylogenetic comparisons with more basal tapiromorph perissodactyls, for example, *Lophiodon* (Holbrook, 2009) and *Colodon* (Colbert, 2005), as it does not require exhaustive character comparisons across all species of tapir through time. However, to test evolutionary questions on the functional morphology of the postcranial skeleton in basal, tetradactyl perissodactyls, a comprehensive understanding of limb variation in potential modern analogues is essential. One such question concerns the true axis of symmetry in the mesaxonic autopodium.

Perissodactyls, including tetradactyl, tridactyl, and monodactyl taxa, possess mesaxonic symmetry in their manus (Klaits, 1972); the axis of symmetry passes through the third digit. The term 'mesaxonic' has been used to describe autopodia in a variety of tetrapod groups. Anatomical and morphometric studies determine a mesaxonic autopodium to exhibit a third digit that is longer than all the others, flanked by digits two and four, which are shorter than digit three but of comparable length to one another (Brown & Yalden, 1973; Lockley, 2009; Rajkumar & Klein, 2014; Reghem et al., 2012; Tougard et al., 2001). Other studies approach the subject of mesaxony from a more functional and biomechanical standpoint, suggesting that mesaxonic symmetry is not exclusively defined by longer third digits, but that the central third digit is loaded most greatly during locomotion. Lateral digits are then loaded approximately equally (Brown & Yalden, 1973; Holbrook, 2001; Klaits, 1972), with the third digit acting as the centre of rotation during lift-off of the foot (Klaits, 1972). The first, anatomical definition of mesaxonic symmetry has been known to be true for perissodactyls for many years (Earle, 1893, 1896; Gregory, 1929; Simpson, 1945); the second, biomechanical interpretation has yet to be explored in all living perissodactyl groups. Understanding the comparative morphology of the manus in modern tapirs, which are known to exhibit anatomical mesaxonic symmetry, may reveal osteological evidence for variation in load application across the four manual digits that also support the biomechanical interpretation of mesaxonic symmetry. Unfortunately the majority of tapir postcranial research has centred on qualitative descriptions, with little by way of quantitative morphological investigation required for proper functional interpretations.

Previous qualitative studies of modern tapir postcranial morphology have revealed interspecific differences, almost exclusively between the lowland tapir, *Tapirus terrestris* L., and the Malayan tapir, *Tapirus indicus* Desmarest (Earle, 1893; Gregory, 1929). Results often align, with *T. indicus* shown to possess longer, heavier, and more graviportally adapted limb elements compared to *T. terrestris* in all analyses (Earle, 1893; Hulbert, 1995; Osborn, 1929). In addition, *T. terrestris* has been stated to have a smaller lateral toe (fifth metacarpal) relative to tapirs of greater body size, for example, *T. indicus*, *T. haysii* Leidy (Earle, 1893; Hulbert, 1995; Osborn, 1929). When interpreted functionally, the graviportal adaptations of the upper arm, carpus and the metacarpals in *T. indicus* have been suggested to imply greater loading on the forelimb, and in turn greater reliance on the lateral digits than the smaller *T. terrestris* (Earle, 1893). Many of these qualitative observations may have functional consequences and also associated changes in surrounding bones which have not yet been quantified.

Quantitative comparisons of tapir postcrania have recently been undertaken, with results suggesting that differences in both forelimb (MacLaren & Nauwelaerts, 2016; Nauwelaerts, Vangeel, & Aerts, 2016) and hindlimb (Hawkins, 2011) pertain to subtle variations in locomotor ecology across extant tapir species. These quantitative studies corroborate qualitative observations on the large Malayan tapir (*T. indicus*), demonstrating that this species exhibits subtle adaptations to the upper forelimb bones consistent with increased necessity for gravitational support (MacLaren & Nauwelaerts, 2016). The mountain tapir (*Tapirus pinchaque* Roulin) has been shown to possess gracile upper forelimb and lower hindlimb bones (Hawkins, 2011; MacLaren & Nauwelaerts, 2016), and morphological features pertaining to proximal shock absorption and increased stride frequency (MacLaren & Nauwelaerts, 2016). The upper forelimb morphologies of the Baird's (*Tapirus bairdii* Gill) and lowland (*T. terrestris*) tapirs have been shown to differ significantly from both *T. pinchaque* and *T. indicus*, despite presenting only subtle osteological differences from one another (corroborating qualitative observations of these species by MacLaren & Nauwelaerts, 2016; Simpson, 1945). From the results of the few quantitative studies on tapir limbs that have been performed, ecological conclusions have been drawn (Hawkins, 2011; MacLaren & Nauwelaerts, 2016; Nauwelaerts et al., 2016). Here, we present a quantitative assessment of the autopodium of extant tapirs to further our understanding of interspecific differences in the locomotor apparatus of modern tapirs.

Using results and interpretations from qualitative studies on the perissodactyl carpus and metacarpus, combined with recent quantitative results on tapir postcranial anatomy (Hawkins, 2011; MacLaren & Nauwelaerts, 2016), we will investigate several hypotheses concerning tapir autopodial variation. First, we will quantitatively test the hypotheses presented by Earle (1893), Osborn (1929), and Simpson (1945), detailing differences in the morphology of the carpals and metacarpals between *T. indicus* and *T. terrestris*. Furthermore, due to its larger average body dimensions and mass (de Thoisy et al., 2014), we hypothesise that *T. indicus* will display shape differences in keeping with greater loading on the autopodium compared to all other extant species across all autopodial bones. Recent work on the limb morphology of modern tapirs has shown distinct morphological differences between the mountain tapir (*T. pinchaque*) and other neotropical tapirs (Hawkins, 2011; MacLaren & Nauwelaerts, 2016); in keeping with these results,

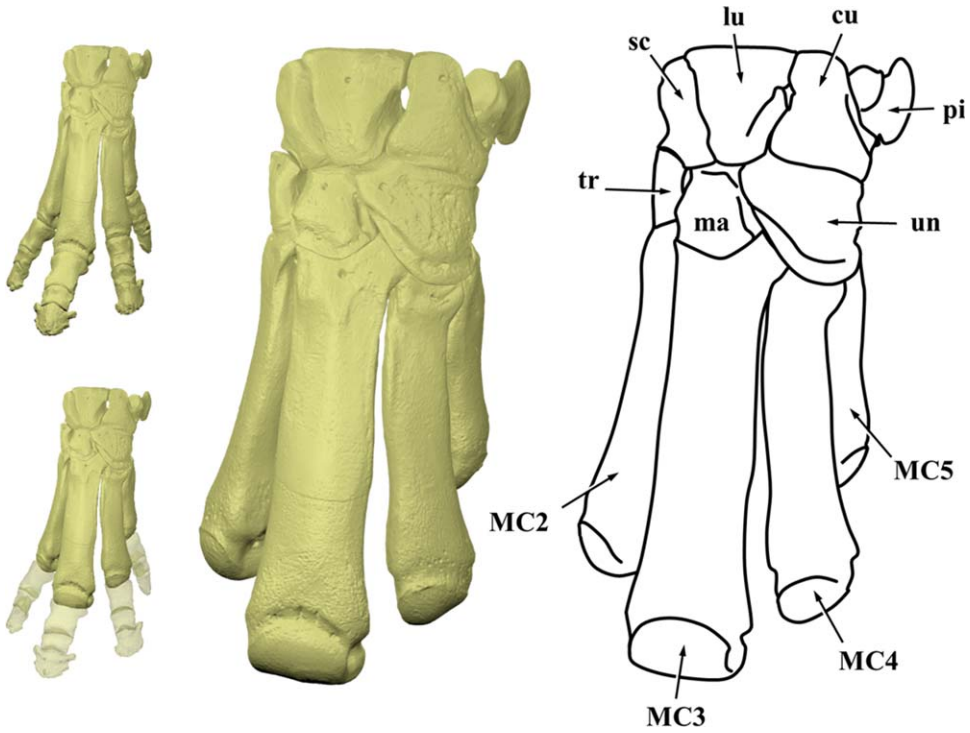

FIGURE 1 Bones of the tapir autopodium. Fully articulated left forefoot (based on scans of RMNH 43495), with enlarged autopodium representing bones used in this study: sc = scaphoid; lu = lunate; cu = cuneiform; pi = pisiform; tr = trapezoid; ma = magnum; un = unciform; MC2 = second metacarpal; MC3 = third metacarpal; MC4 = fourth metacarpal; MC5 = fifth metacarpal

we predict significant differences in the autopodial anatomy of *T. pinchaque* relative to other neotropical tapirs. Finally, we hypothesise that mean average carpal and metacarpal shapes for *T. terrestris* and *T. bairdii* will not show significant differences, based on results from both qualitative (Simpson, 1945) and quantitative (MacLaren & Nauwelaerts, 2016) studies. By testing these hypotheses, we aim to shed light on potential differences in the mesaxonic manus of modern tapirs (Klaits, 1971), and infer biomechanical outcomes based on any variation revealed. We will use discriminant function analyses (DFA) to identify features of the autopodium that contribute to accurate discrimination between species, and aim to formulate functional interpretations from these discriminant features.

2 | MATERIAL AND METHODS

2.1 | Specimens

As study material, 22 disarticulated forelimbs (dry bones) of tapirs were collected from museums in Europe and the United States (see Supporting Information 1 & 2). Four species of modern tapir (*T. terrestris*, *T. pinchaque*, *T. bairdii*, and *T. indicus*) were collected for analysis, with multiple specimens accounting for intraspecific variation. Whenever possible, morphologically mature specimens were scanned (adult; Supporting Information), as defined by the complete ossification of the epiphyses, including the scapular cartilage (Liebich, Konig, & Maierl, 2007; Simpson, 1945). Specimens without fully ossified dorsal borders (subadult; Supporting Information) were also included. Sexual dimorphism has been described as nonsignificant for morphological comparisons in tapirs, and, therefore, was not considered as a limiting factor for specimens (Simpson, 1945). Seven carpals and all four metacarpals were included in the study (Figure 1). Sesamoids and phalanges were not included in this study due to poor sample sizes for these elements. The bones were split into three groupings: the proximal carpal row, distal carpal row, and metacarpals. The proximal row included the pisiform (*accesorium*), cuneiform (*ulnare*), lunate (*intermedium*), and scaphoid (*radiale*). The distal row included the trapezoid (*carpale II*), magnum (*carpale III*), and unciform (*carpale IV*). The trapezium (*carpale I*) was observed in the juvenile *T. indicus* after dissection and is known to be exhibited in living perissodactyls, although with little consistency (Constantinescu et al., 2012); the trapezium was omitted from this analysis as few scanned specimens possessed it or had the bone preserved for study. All available metacarpals (MC2, MC3, MC4, MC5) were included in the analysis (Figure 1).

A dissection was performed on the limbs of a juvenile *T. indicus* to supplement functional interpretations from published tapir osteology and myology (Campbell, 1936; Murie, 1871; Pereira, 2013). The juvenile tapir was provided by the Royal Zoological Society of Antwerp (KMDA). Muscular and ligamentous attachment sites available from the dissection and published literature assisted in the identification of osteological features and interpreting functional outcomes. Veterinary accounts of equid and rhinocerotid osteology and myology (Budras, Sack, & Rock, 2003; Clayton, Chateau, & Back, 2013; Constantinescu et al., 2012; Liebich et al., 2007; Yalden, 1971) were used where necessary to assist identification and interpretations.

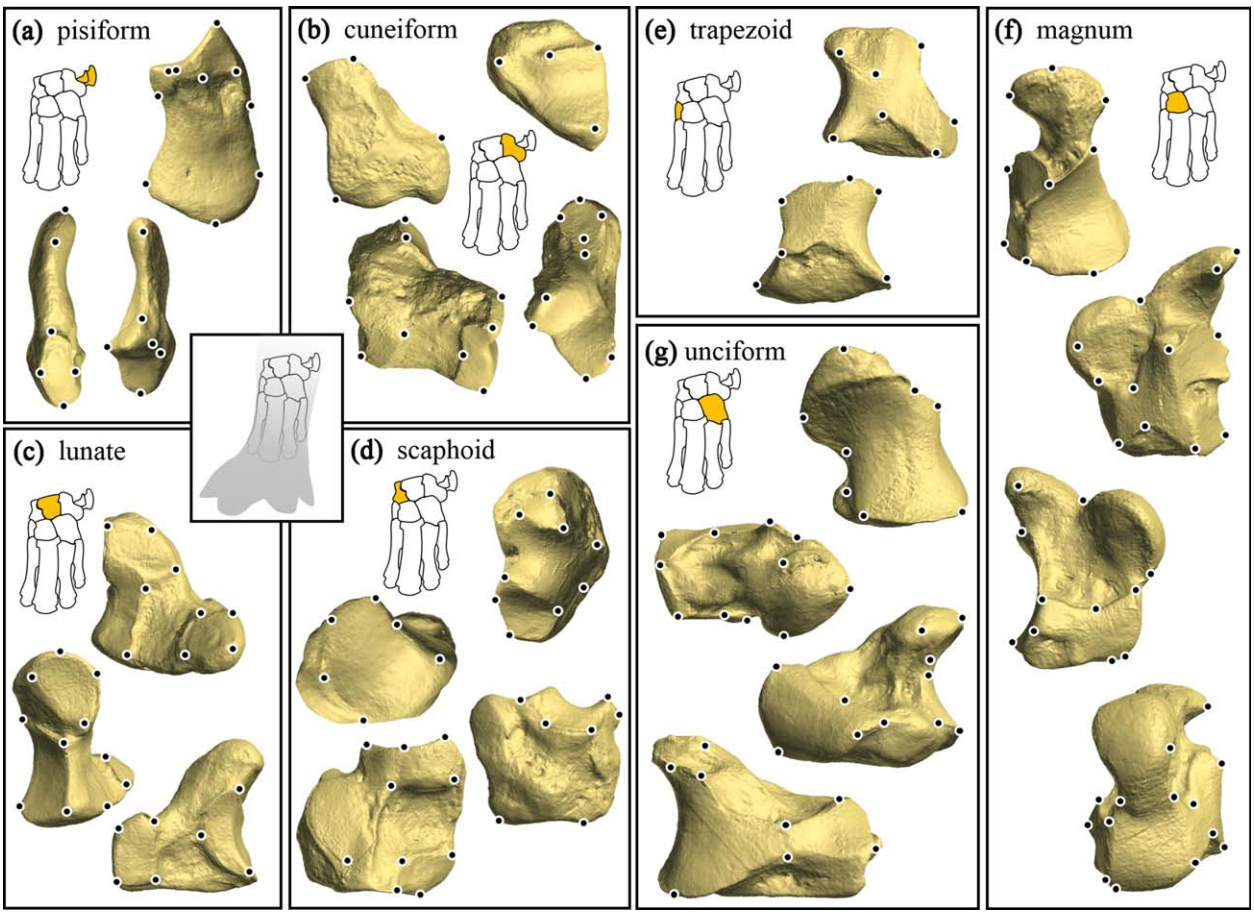

FIGURE 2 Landmark placement on seven bones of the tapir carpus. Proximal row (a)–(d) and distal row (e)–(g). Carpus position in the foot depicted within the grey outline (left). Position of the bone in the carpus relative to other elements demonstrated on each autopodium diagram (orange bone). Specific landmark denomination for each bone can be found in Supporting Information 3. Representative bones from scans of MEO 2203a

2.2 | Scanning

The disarticulated carpus and metacarpals from one forelimb of each specimen were laser scanned using a FARO ScanArm Platinum V2 system with integrated FARO Laser Line Probe (up to 50 μm resolution). Bones were balanced on supports positioned on regions of the specimen surface on which landmarks could not be placed (e.g., shaft of metacarpal). A three-dimensional virtual point cloud was produced for each autopodial bone, visualised in GeoMagic (GeoMagic Qualify v.10, Morrisville, NY). Any outlying surfaces in the point clouds (e.g., incidental scanning of support structures) were digitally removed to focus only on surface information from the bones. Point clouds were then converted into polygon-based surface models, ranging in detail from 200 k to 500 k polygons, dependent upon bone and the detail necessary around articular surfaces.

2.3 | Geometric morphometrics

Landmark-based geometric morphometrics has been extensively used and is an appropriate technique for quantifying differences in shape between three-dimensional objects (Gould, 2014; Rohlf & Slice, 1990). The technique is based on series of discrete, biologically or operationally homologous points (landmarks) placed onto a succession of objects (Zelditch, Swiderski, & Sheets, 2012). Type II landmark points (representing maxima and minima) were used in this study to define the shape of the carpals and metacarpals. Landmark placement on representative bones in this analysis are visualised in Figures 2 (carpals) and 3 (metacarpals). To aid in the description of discriminant features, landmarks were annotated with subscript denominations pertaining to the bone the landmark describes (as in MacLaren & Nauwelaerts, 2016) (defined in Supporting Information 3: Table S1). Surface models were imported into Landmark Editor v.3.0 software (Wiley, et al., 2005) for three-dimensional landmark application. Raw landmark coordinates were then exported into MorphoJ v1.06d (Klingenberg, 2011) and aligned using Generalised Procrustes Analysis (GPA). This technique removed the effect of size, location and orientation, and aligned raw coordinate configurations based on geometric centre (centroid), minimising inter-landmark distance (Adams, Rohlf, & Slice, 2004; Rohlf & Slice, 1990; Zelditch et al., 2012). Resultant Procrustes coordinates and centroid sizes were then exported into SPSS v.23 (IBM Corp., 2013) for discriminant analyses and *post hoc* testing. Centroid size represents an intrinsic size measure that can be used to scale a configuration of

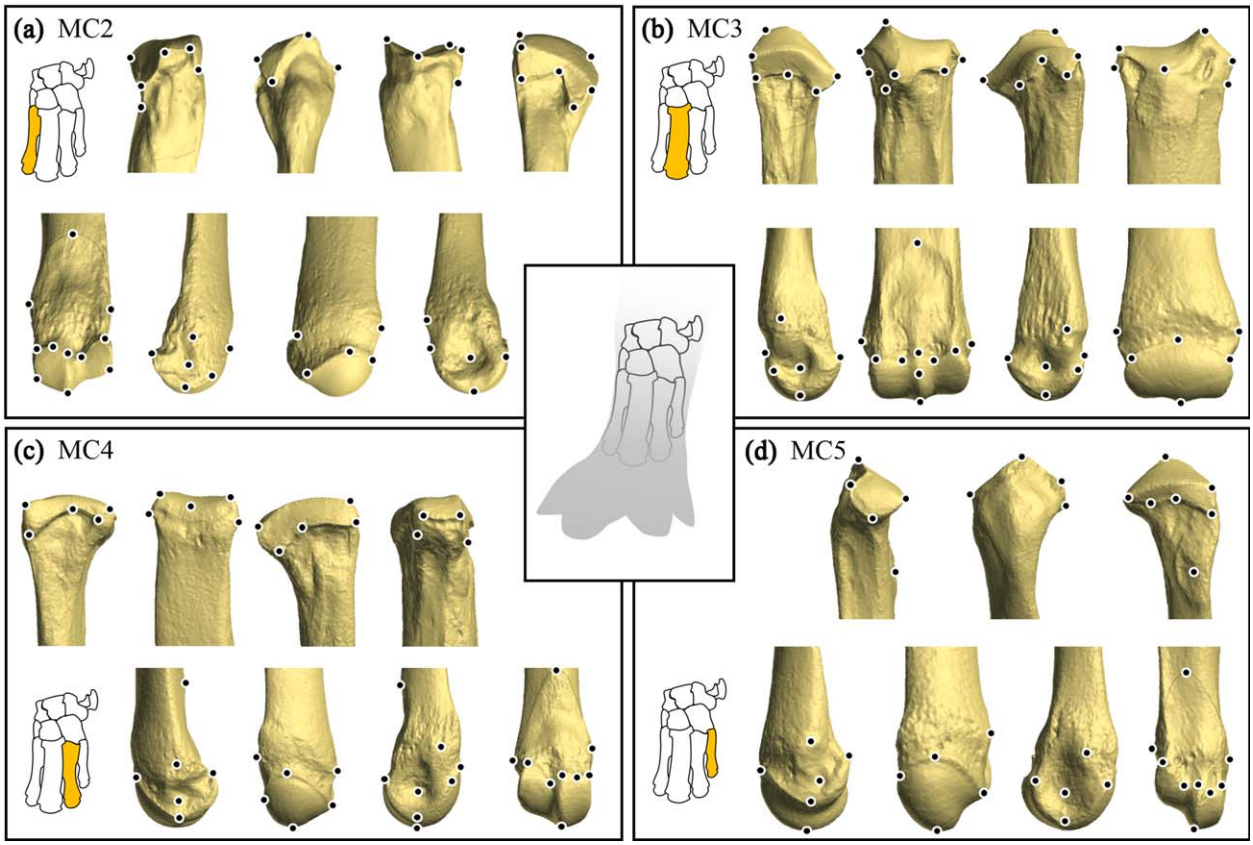

FIGURE 3 Landmark placement on the four tapir metacarpals. (a) metacarpal II, (b) metacarpal III, (c) metacarpal IV, and (d) metacarpal V. Metacarpal position in the foot depicted within the grey outline. Position of each metacarpal relative to other bones portrayed in each autopodium diagram (orange bone). Specific landmark denomination for each bone can be found in Supporting Information 3. Representative bones from scans of MEO 2204b

landmarks, for example, to assess metric distances between landmarks. Centroid sizes for adult specimens were retained for size comparisons. A multivariate analysis of variance (MANOVA) was performed on the Procrustes coordinates calculated for each bone. MANOVA was used to test differences in the means of the groups (species), and the observed power of our MANOVA using small sample sizes was retrieved from the analysis. The MANOVA and power analysis was performed in SPSS v.23.

2.4 | Discriminant function analysis

A linear DFA was performed on the Procrustes coordinates (*x*, *y*, *z*) for all bones. DFA was used to determine what combination of continuous variables for each bone best discriminated between the four species. DFAs were performed in SPSS v.23 (IBM Corp., 2013) using a forward step-wise method for Procrustes coordinate input; this removed independent variables that were not significant for discrimination. A classification table was produced by predicting group membership and cross-validating by jack-knifing the dataset. Sensitivity and specificity tests were also performed. To assess differences in group means, we employed the Wilk's lambda test (0–1; 0 = highest likelihood of inequality, 1 = high likelihood of group means being equal). For visualisation of results, linear discriminant function plots were produced based on the first two discriminant functions (DF1 & DF2), which accounted for the highest percentage of variance. Territorial maps were added to demonstrate how groups were divided and where cut-off values were placed dependent on DF1 and DF2 scores. The third discriminant function accounted for between 0.3% and 11.6% of total variance; DF3 is reported in the results, but is not plotted in discriminant function plots. Cut-off values between groups were based on the weighted mean of the discriminant score for each group centroid. Classification tables and territorial maps were produced in SPSS v.23 (IBM Corp., 2013), and resultant discriminant function plots were configured in R Studio (R Core Development Team, 2008).

2.5 | Partial least squares analysis

Within the carpal complex there are a variety of bones with multiple facets interacting with one another. Changes in morphology in one joint facet which may signal a shift in mechanical capabilities should correspond to similar changes in adjoining bones. In order to assess whether bones and joint facets covary in morphology with neighbouring carpals, we utilised a two-block partial least square analysis (2B-PLS) accompanied by a permutation test (10,000 repetitions) to test for significance of covariance (Fadda & Corti, 2001; Rohlf & Corti, 2000). The RV coefficient of integration (multivariate generalization of

TABLE 1 Jack-knifed classification accuracy for autopodial specimen assignments from linear discriminant analysis

	Specificity				
Autopodial bone	***T. bairdii***	***T. indicus***	***T. pinchaque***	***T. terrestris***	**% Accuracy**
Pisiform	1.00	1.00	1.00	0.80	**94.7**
Cuneiform	0.60	1.00	0.75	0.60	**75.0**
Lunate	1.00	1.00	1.00	0.80	**95.0**
Scaphoid	1.00	1.00	1.00	1.00	**100**
Trapezoid	1.00	1.00	1.00	1.00	**100**
Magnum	1.00	1.00	0.67	1.00	**95.2**
Unciform	1.00	1.00	1.00	1.00	**100**
MC2	1.00	1.00	1.00	1.00	**100**
MC3	1.00	1.00	1.00	1.00	**100**
MC4	1.00	1.00	0.75	0.83	**90.9**
MC5	1.00	1.00	1.00	0.83	**95.5**

Specificity of classification for each bone are presented alongside % accuracy following jack-knifing the dataset.

squared Pearson correlation coefficient; Klingenberg, 2009) produced by PLS analyses is used to predict degree of covariation between two blocks of data (in this case, landmark coordinates and facet areas); it is measured between 0 (no covariation) and 1 (complete covariation) (Klingenberg, 2009). This analysis was used for adjoining carpals which demonstrated key features which both discriminated between species and pertained to possible biomechanical differences during locomotion. When area measurements were tested for covariance (as opposed to landmark coordinates) the raw area data were log-transformed prior to 2B-PLS analysis. The PLS analyses were performed in MorphoJ v1.06d (Klingenberg, 2011), with graphical representations compiled in R Studio (R Core Development Team, 2008).

2.6 | Joint facet comparisons

To compliment carpal shape differences detected using 3D-landmark analysis, the relative areas of joint surfaces were also calculated. Variation in joint surfaces (facets) have been reported in tapirs through qualitative comparisons (Earle, 1893; Osborn, 1929; Simpson, 1945); here we used landmark analyses to detect differences in the shape of facets using only the landmarks that define the joint facet in question. In addition, we calculated relative areas of a series of joint surfaces of the scaphoid, lunate and unciform to quantify previous qualitative claims about interactions between carpals within the autopodium (Earle, 1893; Osborn, 1929; Simpson, 1945). We identified and tested two inter-carpal facet relationships: the distal lunate facet (DLF) ratio (highlighted by Earle, 1893) and the unciform-magnum facet ratio (again pertaining to the lunate, Osborn, 1929; Simpson, 1945). The distal lunate possesses two large facets: anteriorly the unciform facet and posteriorly the volar magnum facet. The anterior magnum facet is found alongside the unciform facet. In the densely packed carpus, a relatively larger facet intuitively implies greater loading rather than greater mobility, with a larger surface area available for force transmission. The three-dimensional scans of the carpal bones provided smooth articular surfaces for quantitative comparison between carpals. Facet areas were calculated by pruning the full 3D-laser scans of bones until only the joint facet under study remained; this was performed in GeoMagic (GeoMagic Qualify v.10, Morrisville, NY). These reduced surface scans were then imported into MeshLab (Cignoni et al., 2008) to calculate surface areas. Ratios were formulated by dividing the posterior or anterior magnum facet area (whichever was appropriate) by the combined total of the unciform joint facet and the respective magnum facets. To test for covariation between the joint facets of the distal lunate (both between anterior unciform-magnum and posterior unciform-magnum), a two-block partial least square analysis (2B-PLS) was performed on the log-transformed area data. 2B-PLS analyses and 10,000 permutations were performed in MorphoJ v1.06d (Klingenberg, 2011).

2.7 | Distal metacarpophalangeal facet variation

The distal metacarpal shape was further investigated using a subset of landmarks to test for interspecific differences exclusively in the distal joint surface. Eight landmarks, homologous for all four metacarpals across tapir species, were selected, describing the palmar distal joint facet (metacarpophalangeal joint). In order to test for differences concurrently between both metacarpals and species, a Procrustes ANOVA was performed in MorphoJ. This analysis was used to complement and inform functional interpretations of morphological changes in the distal metacarpals pertaining to interactions with the proximal phalanges (pastern) and the proximal sesamoids.

3 | RESULTS

Overall, linear discriminant functions successfully discriminated between the four extant species of tapir for all autopodial bones. Jack-knifed classification tables for all bones in the autopodium are

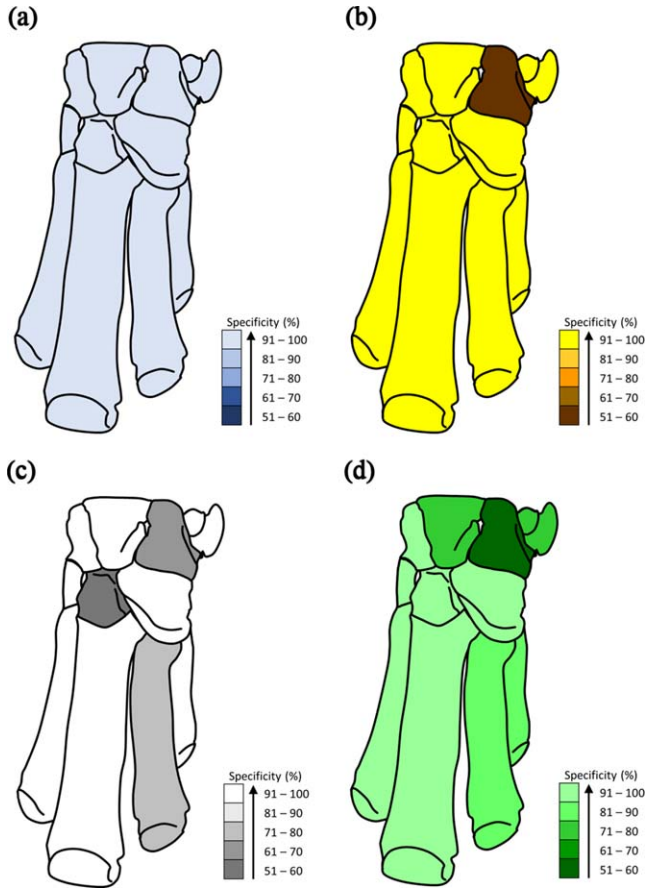

FIGURE 4 Specificity of autopodial discrimination across four tapir species. From top left: (a) *T. indicus*; (b) *T. bairdii*; (c) *T. pinchaque*; (d) *T. terrestris*. Bones of the autopodium shaded to represent the accuracy of classification from Linear Discriminant Analysis. Darker colours represent lower % specificity, with light colours representing high % accuracy of interspecific discrimination. *T. indicus* demonstrates 100% classification accuracy; the cuneiform represents the bone most frequently misclassified across neotropical taxa

presented in Table 1, reporting sensitivity and specificity of the analyses. Accuracy of jack-knifed species classification for autopodials exceeded 75% accuracy for all cases. *T. indicus* is classified 100% accurately for all carpal bones, whereas *T. terrestris* is the most frequently misclassified species (six different bones). *T. bairdii* is the most accurately classified neotropical tapir, with only the cuneiform demonstrating inaccuracy in classification (Table 1). Power analyses revealed high statistical power for all MANOVAs (mean power = 0.88 ± .08); full tabulated results can be found in the Supporting Information 4: Table S2. We are therefore confident in the power of this analysis and the morphological differences between the taxa. Here, we describe results of DFA for all autopodials (proximal carpal row, distal carpal row, and metacarpals). Descriptions of landmarks affecting discrimination can be found in the Supporting Information.

3.1 | Proximal carpal row

The proximal carpal row (scaphoid, lunate, cuneiform, and pisiform; Figure 1) contains the bones that interface with the radius and ulna; the scaphoid, lunate, and cuneiform also articulate with the distal carpal row. Interspecific classification in the proximal carpal row ranges from 100% accuracy (scaphoid) to 75% accuracy (cuneiform; Figure 4), with bones that articulate with the radius (scaphoid and lunate) showing more accurate classification than those articulating with the ulna (cuneiform and pisiform; Table 1). Here, we present results for DFA on the bones of the proximal carpal row:

3.1.1 | Scaphoid

The scaphoid is the largest carpal of the tapir proximal carpal row, and articulates proximally with the radius, medially with the lunate, and distally with the magnum, trapezoid and in some cases the trapezium. The first two discriminant functions (DF1 and DF2) based on scaphoid landmarks account for 97.9% of variance (Supporting Information Figure S1a). The features that most greatly influence accurate species classification include the anteroposterior morphology of the palmar lunate facet ($_{sc}$Lm 20), and the upper margin of the trapezoid-magnum facet, defined by $_{sc}$Lm 11. *T. bairdii* shows the greatest distinction in scaphoid morphology from other tapirs. In *T. bairdii*, $_{sc}$Lm 11 is placed more distally and $_{sc}$Lm 20 is more posterior than in other species. Average species centroid sizes for the scaphoid show that *T. indicus* possess the largest scaphoid, with *T. pinchaque* displaying the smallest (Table 2).

3.1.2 | Lunate

The lunate, or semi-lunar, represents the central carpal in the proximal carpal row. The proximal surface articulates with the radius, medially and laterally it articulates with the scaphoid and cuneiform respectively. Distally the lunate has three articular facets: one to the unciform and two to the magnum (one dorsal, one palmar). Discriminant function 1 accounts for 93.1% of variation (Supporting Information Figure S1b); interspecific discrimination along DF1 is most greatly influenced by placement of $_{lu}$Lm6, the edge of the palmar magnum facet closest to the dorsal facet. Dorsal deflection and elongation of this facet in *T. indicus* brings the DLFs into closer proximity to each other. Proximodistal expansion of the entire dorsal surface of the lunate is observed along DF2 between neotropical taxa (Supporting Information Figure S1b), driven by placement of $_{lu}$Lms 3 & 18. Average centroid sizes differ to those of the scaphoid, revealing *T. indicus* to possess the largest lunates and *T. terrestris* the smallest (Table 2).

3.1.3 | Cuneiform

The cuneiform, triquetrum, or ulnar carpal, is the most lateral bone in the proximal carpal row; it articulates proximally with the pisiform and ulna, medially with the lunate, and distally with the unciform (Figure 1). The cuneiform is the most poorly discriminated bone in the autopodium, with one in four bones being misclassified (Figure 4). The first two discriminant functions describe 92.4% of total variance (Supporting Information Figure S1c). One or more specimens of all neotropical species are misclassified as *T. indicus*, with additional misclassification between *T. bairdii* and *T. terrestris*; the first discriminant function successfully separates only *T. pinchaque* from the other species (Figures S1c; see also Supporting Information 5: Table S3). The most discriminatory feature is the shape of the mediodistal facet articulating with the

TABLE 2 Average centroid sizes per species (± standard deviation) for each bone in the autopodium

Bone		*T. bairdii*	*T. indicus*	*T. pinchaque*	*T. terrestris*
Pisiform	mean	54.73 ± 5.6	64.46 ± 3.3	51.42 ± 5.6	53.55 ± 3.3
	n	*3*	*5*	*3*	*5*
Cuneiform	mean	59.48 ± 1.5	64.81 ± 1.2	54.65 ± 2.4	55.59 ± 5.1
	n	*3*	*6*	*3*	*5*
Lunate	mean	74.09 ± 2.1	83.86 ± 3.0	69.67 ± 1.0	68.40 ± 7.1
	n	*3*	*6*	*3*	*5*
Scaphoid	mean	71.43 ± 2.7	86.83 ± 3.5	68.13 ± 3.5	69.24 ± 6.8
	n	*3*	*7*	*3*	*5*
Trapezoid	mean	37.52 ± 1.6	43.08 ± 2.1	32.28 ± 0.4	34.41 ± 2.4
	n	*3*	*4*	*3*	*5*
Magnum	mean	76.50 ± 0.7	87.01 ± 3.0	70.90 ± 1.3	74.15 ± 4.7
	n	*3*	*7*	*3*	*6*
Unciform	mean	71.61 ± 2.0	79.44 ± 2.8	66.00 ± 0.5	69.52 ± 5.5
	n	*3*	*6*	*3*	*5*
MC2	mean	214.74 ± 9.5	228.14 ± 3.7	218.25 ± 9.5	214.27 ± 9.2
	n	*3*	*7*	*3*	*6*
MC3	mean	256.57 ± 15.0	272.32 ± 7.4	263.21 ± 7.9	256.65 ± 11.5
	n	*3*	*7*	*3*	*6*
MC4	mean	202.86 ± 10.7	218.12 ± 7.0	202.33 ± 7.3	202.03 ± 10.6
	n	*5*	*7*	*3*	*6*
MC5	mean	124.66 ± 5.3	153.21 ± 4.4	130.82 ± 4.3	131.20 ± 9.8
	n	*3*	*7*	*3*	*6*

Mean average and standard deviation are reported for each species. Centroids based on full adult specimens (excluding subadults), with number of adult specimens for each bone also listed (*n*).

lunate ($_{py}$Lm 3); the orientation of the cuneiform (defined by $_{py}$Lm 3 and 4) also contributes to successful discrimination of *T. pinchaque*. Average centroid sizes for the cuneiform show a similar pattern to that of the scaphoid, with *T. indicus* displaying the largest and *T. pinchaque* the smallest cuneiform carpals (Table 2).

3.1.4 | Pisiform

The pisiform, or accessory carpal, is the most palmar bone in the carpus and facilitates the passage of flexor tendons through the carpal tunnel. The pisiform articulates distally with the cuneiform and proximally via two facets with the ulna. The first two discriminant functions describe 89.1% of variance, with each species occupying a discrete region of canonical variate-space (Supporting Information Figure S1d). Placement of $_{pi}$Lm 4 (distal extremity of ulnar facet) shows variation along DF1, with *T. indicus* displaying a distinct morphology from *T. bairdii*. DF2 discriminates between *T. terrestris* and *T. pinchaque* with the placement of $_{pi}$Lm12 (accessory ulnar facet) discriminating between these two taxa. As with the scaphoid and cuneiform, *T. indicus* demonstrates the largest centroid sizes for the pisiform, and *T. pinchaque* the smallest centroid size (Table 2).

3.2 | Distal carpal row

The distal carpal row (trapezoid, magnum, unciform) is the most successfully classified group of autopodials (mean classification accuracy = 98.4%). Within this grouping, both the trapezoid and unciform achieved 100% interspecific classification, whereas the magnum was classified with 95.2% accuracy. Graphical results are presented in Supporting Information Figure S2.

3.2.1 | Trapezoid

The trapezoid, or second carpal, is the smallest carpal in the tapir autopodium. It has a proximal articulation with the scaphoid, a lateral facet for the magnum, a distal facet for the second metacarpal (MC2) and a small medial facet for articulation with the trapezium (first carpal; not present in all specimens and, therefore, not included in the analysis). The first discriminant function accounts for 93.6% of interspecific variation, and successfully discriminates the four taxa (Supporting Information Figure S2a). Separation along this function is influenced by the landmarks describing the palmar region ($_{tr}$Lm 7) and the laterodistal margin ($_{tr}$Lm 10) of the of the magnum facet. The difference in the

magnum facet morphology is greatest between *T. bairdii* and *T. indicus*. The centroid size for the trapezoid mirrors that of the scaphoid, cuneiform, and pisiform (Table 2).

3.2.2 | Magnum

The magnum, capitate, or third carpal, is the central carpal of the tapir autopodium. The magnum articulated proximally with the scaphoid and lunate (via two facets), proximolaterally with the unciform, medially with the trapezoid and distally with a small facet for the second metacarpal (MC2) and a large facet for the third metacarpal (MC3). The first discriminant function accounts for 95.8% of magnum variation (Supporting Information Figure S2b). *T. indicus* and *T. bairdii* are the most easily discriminated taxa along DF1; however, specimens of *T. pinchaque* and *T. terrestris* are misclassified along DF1. Landmarks that most heavily influence interspecific discrimination along DF1 include $_{ma}$Lm 7 (expansion-contraction of the unciform facet) and $_{ma}$Lm 15 (defining the concavity of the dorsal trapezoid facet). *T. bairdii* exhibits a highly concave trapezoid joint plane. As with the majority of the carpals (excluding the lunate), *T. indicus* displays the largest average magnum centroid size and *T. pinchaque* exhibits the smallest (Table 2).

3.2.3 | Unciform

The unciform, hamate or fourth carpal, is the largest carpal in the distal carpal row; it articulates proximally with the lunate and cuneiform medially with the magnum, and distally with the third, fourth, and fifth metacarpals (MC3, MC4, & MC5). The first two discriminant functions describe 88.4% of total variance (Supporting Information Figure S2c). The placement of taxa along DF1 is greatly affected by $_{ha}$Lm 3 (lateral morphology of the MC5 joint facet) and $_{ha}$Lm 10 (anteroposterior expansion or constriction of the lunate facet). *T. indicus* displays an expanded lunate-cuneiform facet relative to neotropical taxa. DF2 (32.9%) is most greatly influenced by $_{ha}$Lm 8, which tracks a relative expansion of the medial edge of the cuneiform facet. DF2 is also influenced by $_{ha}$Lm 5, which describes the antero-posterior constriction (*T. bairdii*) and expansion (*T. indicus* and *T. pinchaque*) of the MC4 facet, and by extension the entire distal unciform. The average centroid size is once again greatest in *T. indicus* and smallest in *T. pinchaque* (Table 2).

3.3 | Metacarpals

Overall results for the metacarpals suggest that the lateral bones exhibit marginally less interspecific variation than the medial metacarpals. Mcs 2 and 3 were classified 100% accurately after jack-knifing, whereas Mcs 4 and Mc 5 exhibited occasional misclassification. Centroid sizes for the metacarpals do not follow the same pattern as in the carpals.

3.3.1 | Metacarpal 2

Metacarpal 2 (MC2), or the second metacarpal, is the most medial hand bone in the tapir autopodium. It has a proximal articulation with the trapezoid and trapezium (absent in this analysis), a lateral articulation with MC3, and a distal articular facet for the proximal phalange and proximal sesamoids. DF1 accounts for 99.8% or variation, with *T. indicus* greatly separated from the neotropical taxa (Supporting Information Figure S3a). Separation along DF1 is heavily influenced by the placement of 2Lm 26 (palmar margin of trapezoid facet), and also 2Lms 4 & 5, which describe the morphology of the proximolateral sesamoid joint facet, in addition to affecting the dorsopalmar depth of the metacarpal head. The largest average centroid size for the MC2 is found in *T. indicus*, with the smallest exhibited by *T. terrestris*. *T. pinchaque* exhibits the second largest MC2 centroid size (Table 2).

3.3.2 | Metacarpal 3

Metacarpal 3 (MC3), or the third metacarpal (cannon bone in equids) is the largest metacarpal in the tapir autopodium. Proximally it articulates with the trapezoid, magnum and unciform, proximomedially with MC2, and proximolaterally with MC4; MC3 articulates distally with the proximal sesamoids and phalange for digit three. The first two discriminant functions account for 92.0% of variation (Supporting Information Figure S3b). Landmarks that contribute most greatly to interspecific classification along DF1 include $_{3}$Lm 19 (proximodistal depth of the magnum facet) and $_{3}$Lm 23 (palmar edge of the MC2 joint facet). Classification along DF2 is dominated by $_{3}$Lm 17 (describing the breadth of the unciform joint facet). Average centroid size for MC3 suggests that *T. indicus* have the largest metacarpal; both *T. terrestris* and *T. bairdii* display very similar average centroid sizes, smaller than the other two species (Table 2).

3.3.3 | Metacarpal 4

Metacarpal 4 (MC4), or the fourth metacarpal, is the intermediate metacarpal between the central third and lateral fifth. MC4 articulates with the unciform proximally, MC3 proximomedially, and MC5 proximolaterally; as with other metacarpals, MC4 distally articulates with the corresponding proximal phalange and paired sesamoids. MC4 is accurately classified for 90.9% of specimens (Table 1), with the first discriminant function accounting for 94.8% of variation (Supporting Information Figure S3c). The landmarks which contribute most greatly toward interspecific discrimination describe the concave shape of the unciform facet ($_{4}$Lm 15) and the expansion-contraction of the medial margin of the metacarpophalangeal joint facet ($_{4}$Lm 8). The MC4s of the neotropical tapirs show very similar average centroid sizes, with *T. terrestris* marginally displaying the smallest (Table 2).

3.3.4 | Metacarpal 5

The fifth metacarpal (MC5) is the most lateral hand bone, and the smallest metacarpal in the tapir autopodium. Proximally MC5 articulates with the unciform, proximomedially with MC4, and distally with the proximal phalange and paired sesamoids of digit five. The first two discriminant functions account for 94.5% of interspecific variation. Along DF1, three morphotypes are separated (Supporting Information Figure S3d). Landmarks that display high loading on DF1 include those describing the morphology of the lateral sesamoid facet ($_{5}$Lms 3 & 5), which divides modern tapirs into three morphotypes (Supporting Information Figure S3d). *T. bairdii* displays a notably smaller average

TABLE 3 Procrustes ANOVA significance test results for subset of landmarks describing metacarpophalangeal facet of Mc2, Mc3, Mc4, and Mc5 across four tapir species

Variable	Sum of squares	Mean squares	df	*F*	Parametric *p*-value
Species	.0839	.001645	51	3.38	**<.01**
Metacarpal	0.9891	.019394	51	39.81	**<.01**

Bold values denote significant differences.

centroid size than other neotropical taxa, with T. indicus exhibiting the largest average centroid size for MC5 (Table 2).

3.3.5 | Metacarpophalangeal facet

The metacarpophalangeal joint of the tapir metacarpal comprises of three principal regions: the medial sesamoid facet, lateral sesamoid facet, and metacarpal sagittal ridge. The subset of eight landmarks describe the proximopalmar margin of the metacarpophalangeal joint, incorporating the sesamoid facets and sagittal ridge. Results for the subset of eight landmarks for all four metacarpals demonstrated notable interspecific differences. Procrustes ANOVA results detected significant differences ($p < .01$) between individual species and between the four metacarpals in the morphology of the distopalmar metacarpal facet (Table 3).

3.4 | Joint facet ratios

3.4.1 | Unciform–magnum facet ratio (UMF ratio)

The unciform-magnum facet ratios show a different pattern to that of the DLFs. *T. pinchaque* displays the largest average anterior magnum facet, and shows a significant difference to *T. indicus* in the ratio of unciform to anterior magnum facets ($p = .014$; Table 4). *T. indicus* displays the greatest range of ratios, with one outlying specimen exhibiting a ratio comparable to *T. pinchaque* (Figure 5). *T. indicus* displays no significant difference to *T. terrestris*, and *T. bairdii* and *T. terrestris* display similar HMF ratios. Covariation analyses based on 2B-PLS analysis of the unciform and anterior magnum facet areas do not support covariation between these facets. PLS1 axes account for 100% of covariation; however, PLS axes do not correlate highly (RV = 0.363; Figure 7a; Table 6). Overall correlation is weak and not statistically significant after permutation (RV = 0.132; $p = 0.117$).

TABLE 4 Tukey-HSD significance test results from one-way ANOVA of hamate-magnum facet area ratios

	Species			
	T. indicus	*T. bairdii*	*T. pinchaque*	*T. terrestris*
T. indicus		0.731	**.014**	0.668
T. bairdii	0.731		0.110	1.000
T. pinchaque	**.014**	0.110		0.131
T. terrestris	0.668	1.000	0.131	

Bold values denote significant differences.

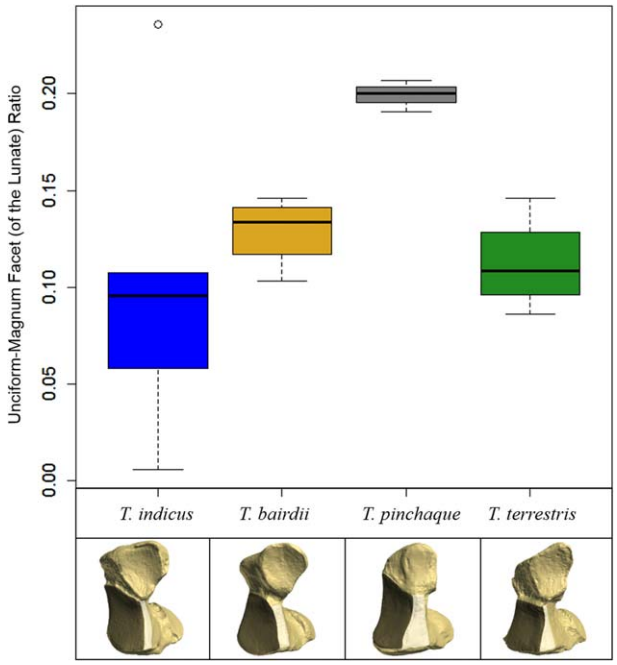

FIGURE 5 Ratio of areas for unciform (dark grey) and anterior magnum (white) facets of the lunate (intermediate carpal). Box plots represent intraspecific variation, with black bar highlighting the mean value; open circles represent outlying specimens. Representative bones (nearest to mean facet value) and ratios: *T. indicus* (RMNH 17923; .09), *T. bairdii* (MVZ 141173; 0.13), *T. pinchaque* (MNHN 1982–34; 0.21), *T. terrestris* (RMNH 12827; 0.15)

3.4.2 | Distal lunate facet ratio (DLF ratio)

The comparison between the DLFs show that there is a spectrum of variation across neotropical species (Figure 6). *T. bairdii* demonstrates the greatest difference between anterior and posterior distal facets (Figure 6), showing a significant difference to *T. terrestris* (Table 5) which exhibits the smallest difference between facet areas. *T. indicus* and *T. pinchaque* demonstrate near identical mean values for distal facet area ratios (*T. indicus*: 0.663 ± .036; *T. pinchaque*: 0.663 ± .031). Covariation analyses based on 2B-PLS analysis of the unciform and posterior magnum facet areas support a covariation relationship between these facets. Again, PLS1 axes account for 100% of covariation, with a strong positive co-relationship between PLS axes (RV = 0.738; Figure 7b; Table 6). Overall correlation is fairly strong (RV = 0.545) and statistical significance from the permutation test is very high ($p < .001$).

3.5 | Partial least squares analyses (2B-PLS)

Results from DFA suggest bones along the medial autopodium (scaphoid, trapezoid, and MC2) are most accurately discriminated across all tapir species (Figure 4). To investigate specific articulations in the medial autopodium, 2B-PLS was performed between the trapezoid and magnum (examining the joint facet between the two bones) and the respective facet morphologies of the trapezoid and scaphoid. Overall 2B-PLS analyses between the trapezoid and magnum revealed a strong

TABLE 6 Two-block partial least squares analysis results for pairwise comparisons between key joint articulations

Facet combination (*n*)	PLS axis	% covar.	*r*	*p*	RV	*p*-value
Unciform-Magnum (*20*)	PLS1	100.0	0.363	0.117	**0.132**	**0.117**
DLFs (*20*)	PLS1	100.0	0.738	<.001	**0.545**	**<.001**
Trapezoid-Magnum (*17*)	PLS1	80.7	0.937	<.001	**0.778**	**<.001**
	PLS2	12.7	0.892	.006		
T. indicus (*4*)	PLS1	78.5	0.959	0.259	**0.915**	**.086**
T. baridii (*5*)	PLS1	71.6	0.978	0.205	**0.667**	**0.446**
T. pinchaque (*3*)	PLS1	86.3	0.999	0.170	**0.992**	**0.170**
T. terrestris (*5*)	PLS1	93.3	0.992	.009	**0.931**	**.009**
Trapezoid-Scaphoid (*15*)	PLS1	60.6	0.903	.005	**0.415**	**.089**
	PLS2	19.5	0.727	0.205		

Number of covariance occurrences per combination tested (*n*), PLS axes accounting for the greatest covariance are included with % accounted for, correlation coefficient (*r*) and significance (*p*) for those axes are presented. Bold RV coefficient of integration and *p*-values represent overall results for the covariation analysis. Species specific comparisons are presented for trapezoid-magnum facet.

covariation in joint facet morphology (RV = 0.778), with high statistical significance from permutation test ($p < .001$). The fist PLS axes account for over 80% of covariance between the bones (Figure 7c; Table 6), which is also highly significant following permutation testing ($p < .001$). Coordinates which most greatly influence covariation for PLS1 include $_{tr}$Lm8 (anterior concave edge of magnum facet), $_{ma}$Lm14, and $_{ma}$Lm15 (anterior and posterior concave margins of trapezoid facet).

The overall 2B-PLS analyses between the trapezoid and scaphoid shows modest covariation in joint facet shape (RV = 0.415), albeit with no statistical significance after permutation test ($p = .089$). The fist PLS axes account for over 60% of covariance between the bones (Figure 7d; Table 6), which does exhibit high statistical significance with permutation testing ($p = .005$). Procrustes coordinates which most greatly influence covariation for PLS1 include $_{tr}$Lm3, 4, and 6 (proximal extremities of both anterior and posterior margins), and $_{sc}$Lm11 and $_{sc}$Lm13 (anterior margin of trapezoid facet and deepest point on the concave facet for the trapezoid).

4 | DISCUSSION

Variation in the carpal and metacarpal arrangement within Perissodactyla has been studied with various qualitative techniques, with both morphological and functional conclusions being drawn at the genus level (*Tapirus*) (Earle, 1893; Holbrook, 2001; Klaits, 1972; Osborn, 1929; Simpson, 1945). However, the comparative morphology and interspecific variation within the manus of the genus *Tapirus* has only briefly been touched upon in previous studies (Earle, 1893; Osborn, 1929; Simpson, 1945), and has not taken all extant taxa into account. Interspecific variation in tapir autopodials may reflect subtle variation

TABLE 5 Tukey-HSD significance test results from one-way ANOVA of DLF area ratios

	Species			
	T. indicus	*T. bairdii*	*T. pinchaque*	*T. terrestris*
T. indicus		0.249	1.000	0.134
T. bairdii	0.249		0.324	**.004**
T. pinchaque	1.000	0.324		0.199
T. terrestris	0.134	**.004**	0.199	

Bold values denote significant differences.

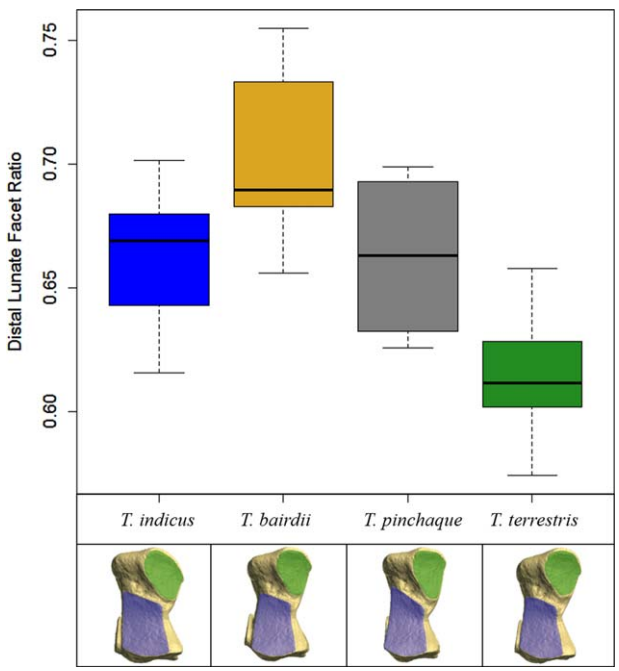

FIGURE 6 Ratio of areas for distal facets of the lunate. Box plots represent intraspecific variation, with black bar highlighting the mean value. Representative bones warped mean landmark configurations applied to RMNH 43495. Facets highlighted on representative bones: anterior distal facet (to proximal unciform; blue); posterior distal facet (to volar process of magnum; top)

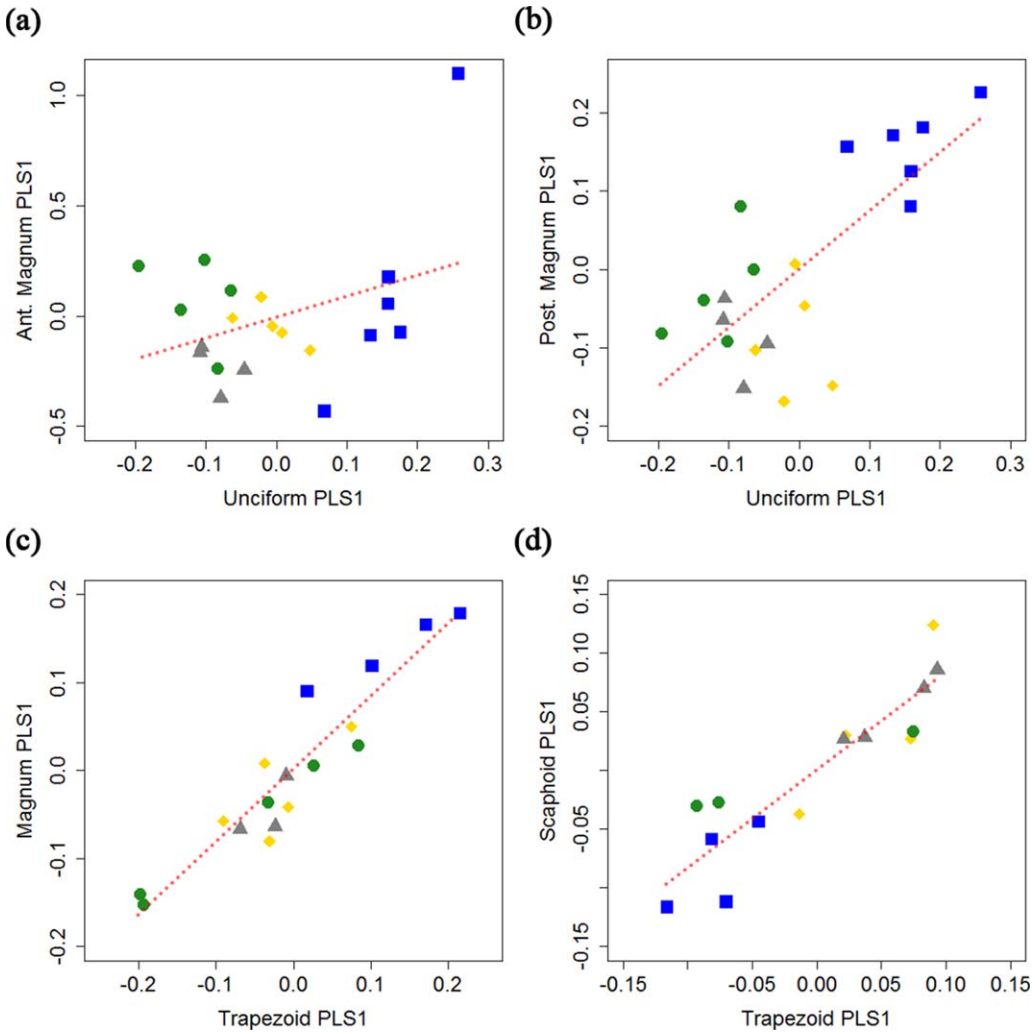

FIGURE 7 Results of 2B-PLS regression analyses comparing (a) unciform and anterior magnum facet area, (b) DLF areas, (c) trapezoid and magnum articulation facets, and (d) trapezoid and scaphoid articulation facets. Symbols: *T. indicus* (squares), *T. bairdii* (diamonds), *T. pinchaque* (triangles), and *T. terrestris* (circles); dotted line denotes line of best fit for all data-points. Statistical data for these plots can be found in Table 6

in locomotor style, and possibly variation in application of loading forces on the anatomically mesaxonic manus of tapirs. Here, we discuss the major osteological differences in the autopodium of extant *Tapirus*, and their implications for locomotor variability in this group.

4.1 | Facets of the lunate

Throughout previous comparisons between tapir postcrania, several key differences in the autopodium have been postulated. In particular, clear differences between *T. indicus* and other modern tapirs have been suggested (Earle, 1893; Osborn, 1929). We find strong support for this distinction between *T. indicus* and other modern tapirs. However, our findings do not correlate with the specific conclusions from previous qualitative studies (Earle, 1893; Osborn, 1929). For example, Earle (1893) noted little to no contact between the lunate and magnum (Figure 1) in *T. terrestris* when compared to *T. indicus*, and that the approximately equal facets for unciform and magnum in *T. indicus* allows equal transmission of force to the medial and lateral digits (Earle, 1893).

Our investigation reveals that the lunate contact with the magnum in *T. indicus* possesses the smallest facet (on average) relative to the unciform joint (Figure 5), which is in direct contrast to the findings of Earle (1893). A relatively larger unciform facet on the lunate would conceivably enable greater force transmission to the unciform and the digits beneath it (the lateral digits) in *T. indicus*. As such, our results for the lunate facets suggest that *T. indicus* may not exhibit biomechanical mesaxonic symmetry, in favour of increased loading on lateral digits. Additionally, results for *T. terrestris* suggest no significant difference to *T. indicus* in the DLFs (Figure 5; Table 3), which also contrasts with Earle's findings. Finally, we found no statistically significant support for covariation between the areas of these facets across the four tapir species. Individual variation in facet size may be a key factor here, as demonstrated by the large error bars for this ratio in *T. indicus* (Figure 5). These findings lead us to conclude that, contrary to the deductions of Earle (1893), tapirs with an enlarged unciform facet will not necessarily display reduction in their anterior magnum facet.

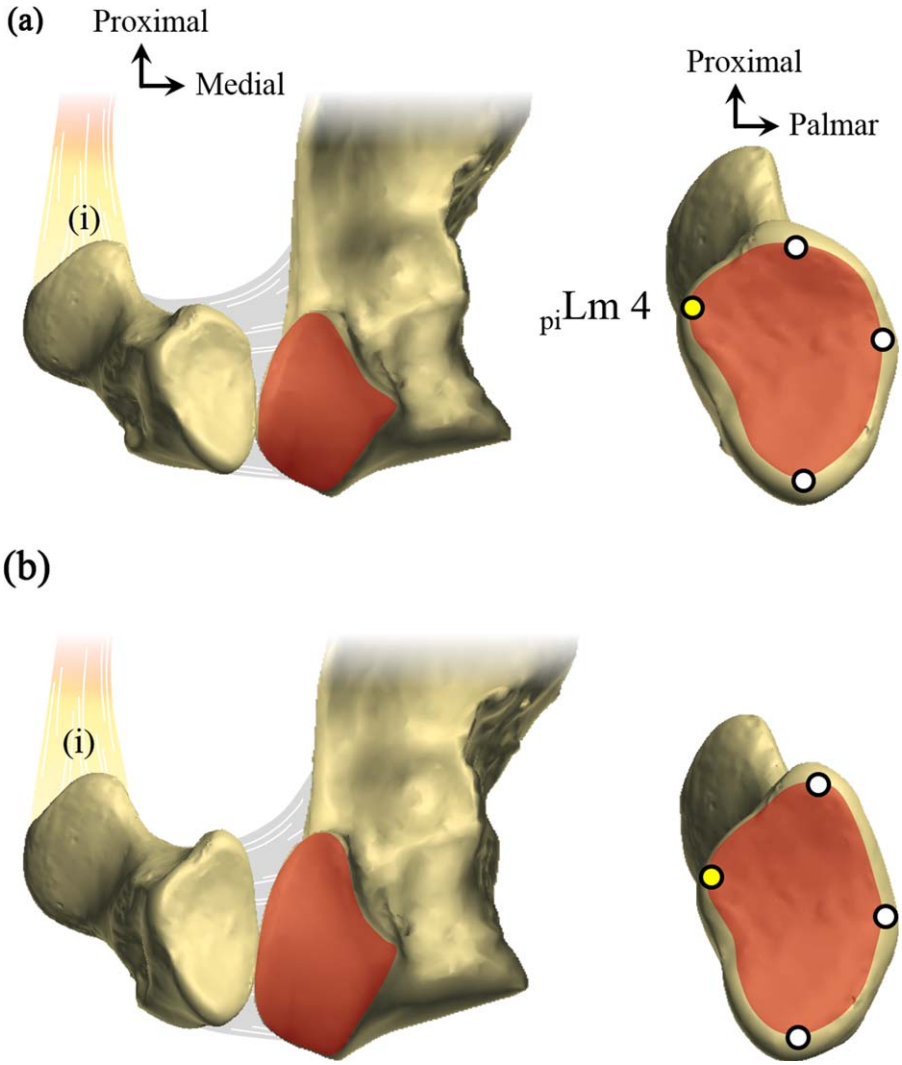

FIGURE 8 Comparison of pisiform-ulna articular morphology in *T. terrestris* (a) and *T. pinchaque* (b). Ulnae scaled to same size. Shaded areas on both ulnae and pisiforms represent articular surface. Ulnae and pisiform depicted in posterior view (pisiform reflected from joint facet; pisiform with landmarks depicted from dorsolateral view. Approximate placement of *m. flexor carpi ulnaris* insertion (i) and carpal retinaculum (grey; connecting pisiform and ulna) is shown. $_{pi}$Lm 4 represents landmark most heavily affecting classification along DF 1 for pisiform. Bones represented depict average morphology for *T. terrestris* and *T. pinchaque* applied to scans of MNHN 1982–34

Our study suggests that *T. pinchaque* exhibits the largest anterior magnum facet of the lunate (Figure 5), which combined with a large unciform facet enables a more even spread of loading forces to the anterior carpal row and both MC3 and MC4. Although, we find no statistical evidence that there is a strong correlation between these facets in our sample, a morphological similarity to extinct tetradactyl perissodactyls is nevertheless present. The carpal arrangement is reminiscent of early, functionally tetradactyl perissodactyls (e.g., *Lophiodon* & *Hyrachyus*) (Osborn, 1929), and supports quantitative results from scapulohumeral morphology suggesting *T. pinchaque* displays a number of osteological features in common with Eocene perissodactyls (MacLaren & Nauwelaerts, 2016). It should also be emphasised that our results for the DLFs and anterior magnum-unciform ratios suggest only very small differences in overall area (~10% between largest and smallest). However, we did find significant covariation in the DLFs, suggesting that the lunate articulation with the posterior magnum is linked to changes in area of unciform facet and *vice versa*. We believe that extrapolating differences in loading regime and further functional outcomes from these small differences would involve over-interpretation of the data. We also stress that the morphological conclusions from Earle (1893) and Osborn (1929) remain on the whole accurate, although their functional interpretations require rigorous re-examination (as recommended by Klaits, 1972) with modern quantitative kinematic methods before any solid conclusions on locomotor function can be made.

4.2 | Mobility of the pisiform

The accessory carpal (pisiform) of tapirs is flattened dorsopalmarly and curves inwards toward the medial border of the autopodium. The curvature of the pisiform enables the passage of the flexor tendons of the

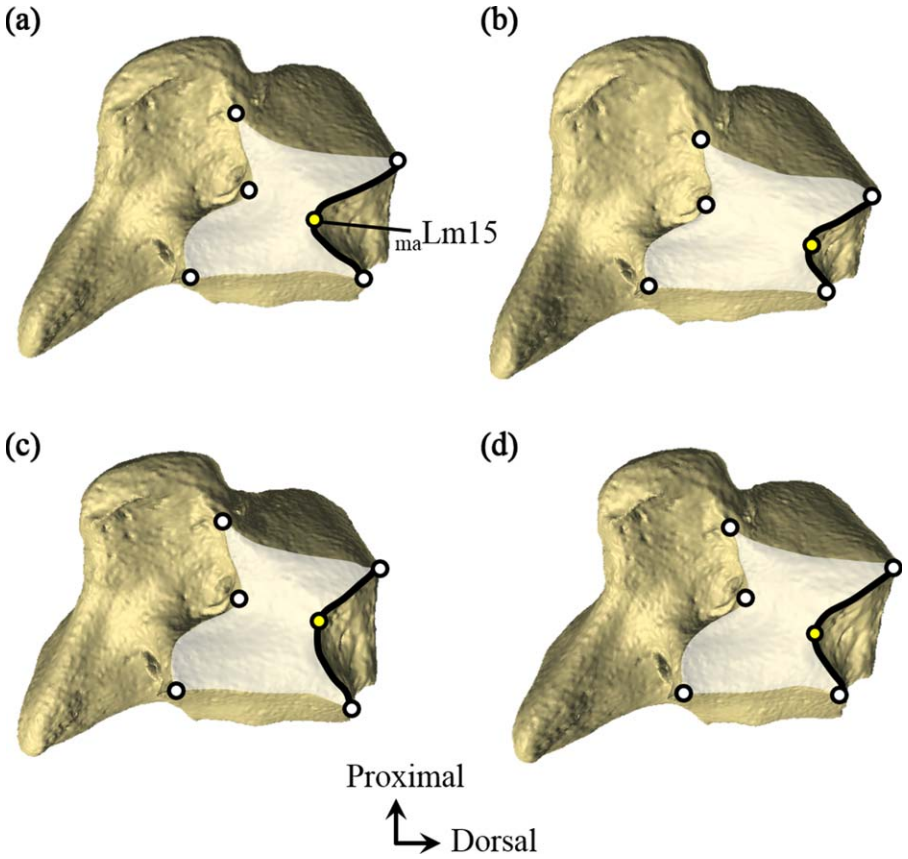

FIGURE 9 Comparison of trapezoid (second carpal) facet morphology of the magnum (third carpal) in extant *Tapirus*. Medial view. From top left: (a) *T. bairdii*; (b) *T. indicus*; (c) *T. pinchaque*; (d) *T. terrestris*. Representative facet areas shaded and outlined with landmarks (white circles) used in morphometric analysis; $_{ma}$Lm 15 (yellow circle) highly discriminatory along DF 1 for magnum. Concave dorsal margin of trapezoid facet marked in bold black

m. flexor digitorum sublimis + *profundus* through the carpal tunnel (Bressou, 1961; Campbell, 1936; Murie, 1871), and the spatulate tip of the bone is the site for attachment of the *m. flexor carpi ulnaris* (proximal) and *m. abductor digiti minimi* (distal). A recent quantitative analysis revealed two different morphologies for the pisiform facet of the ulna in *Tapirus* (MacLaren & Nauwelaerts, 2016); *T. terrestris* and *T. indicus* demonstrated mediolaterally broad pisiform facets on the posterior ulna, whereas *T. bairdii* and *T. pinchaque* exhibited more proximodistally elongate facets. Results from the present analysis of the pisiform (accessory carpal) suggest a similar pattern of morphological disparity, especially between *T. terrestris* and *T. pinchaque* (Figure 8), further corroborating previous analyses revealing differences in forearm osteology between these closely related taxa (MacLaren & Nauwelaerts, 2016). In *T. terrestris*, the pisiform facet is sub-rhomboidal with approximately parallel edges, and the articulating facet of the ulna is semi-circular in lateral view (Figure 8a; also MacLaren & Nauwelaerts, 2016). This offers the pisiform of *T. terrestris* a relatively smaller surface with which to articulate compared to the other neotropical tapirs, while concurrently allowing a greater range of mobility for the pisiform during carpus flexion. The flatter, more elongate pisiform facet for the ulna may limit the functional capabilities of the lateral autopodium in *T. pinchaque* and *T. bairdii*, whereas *T. terrestris* does not appear to be under such mechanical constraints. In addition, the insertion area for the *m. flexor carpi ulnaris* on the proximoposterior edge of the pisiform (Figure 8i) is accentuated in neotropical taxa (most greatly so in *T. bairdii*), whereas *T. indicus* shows no great proximal expansion. The prominent insertion point in neotropical taxa offers a greater surface area for tendon attachment, suggesting increased resistance to carpal overextension (by the antagonistic *m. flexor carpi ulnaris*). By contrast, the broader distal edge of the pisiform in *T. indicus* offers greater attachment surface for the *m. abductor digiti minimi* (abductor of the fifth digit) (Campbell, 1936; Murie, 1871). In addition to an enlarged attachment site for the *m. adductor digiti minimi* on the volar process of the magnum, this morphological feature implies that *T. indicus* has greater muscular control over the fifth digit, allowing it to splay the toes to support greater mass on soft substrates. This result supports previous claims that *T. indicus* utilises the fifth digit to a greater extent than its living neotropical relatives (Earle, 1893; Gregory, 1929). To assess whether this morphology is common to all large tapir species, similar analyses on extinct taxa of high estimated body mass (e.g., *T. haysii*, *T. augustus*) will be necessary.

4.3 | Medial digit loading

Typically, the lateral and medial digits within a mesaxonic autopodium will be loaded approximately equally (Holbrook, 2001; Klaits, 1971).

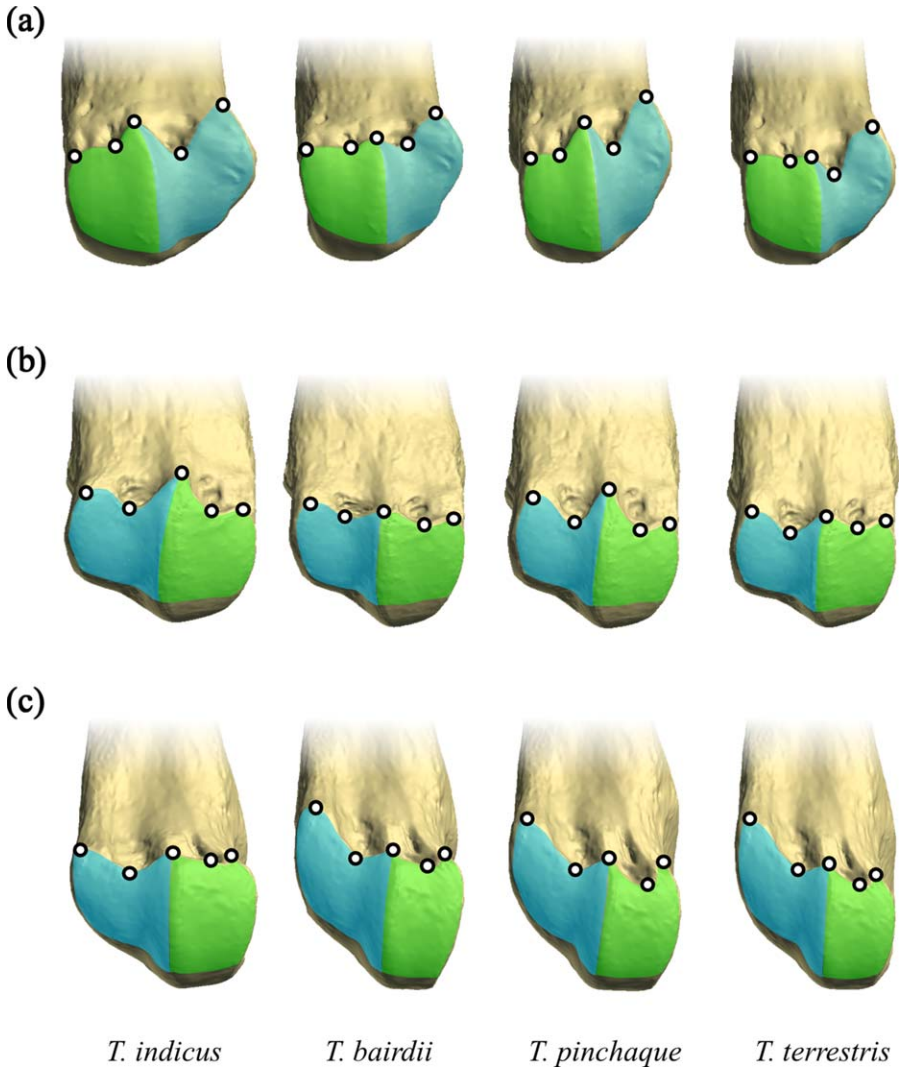

FIGURE 10 Comparison of the morphology of the palmar metacarpophalangeal joint facet in extant *Tapirus*. Medial and lateral metacarpals represented: (a) MC2; (b) MC4; (c) MC5. Shaded regions represent approximate facet surface for articulation with the proximal sesamoids either side of the palmar sagittal ridge: green = medial sesamoid; blue = lateral sesamoid. White circles = landmark placement on palmar metacarpophalangeal joint. Average landmark configurations warped onto metacarpals of MEO 2204e

The lateral digits and corresponding unciform (fourth carpal) have been shown to display morphological differences in modern tapirs; therefore, corresponding morphologies in the trapezoid (second carpal) may be expected. One of the most discriminatory features of the trapezoid was the morphology of the joint facet with the magnum (third carpal). The corresponding facet on the magnum was also highly discriminatory (visualised in Supporting Information Figure S2b). For simplicity, we discuss the articulation from here as the trapezoid-magnum facet. The anterior border of the facet is highly concave in *T. bairdii*, affording relatively less surface for articulation between the bones in this species (Figure 9a). By contrast, *T. indicus* displays a much less concave anterior or posterior border to the facet, enlarging the relative area of the facet (Figure 9b). This morphology is mirrored in the trapezoid, and the relationship is strongly supported with results from PLS analyses for covariance. Landmarks defining the concave margins of the facet on both trapezoid and magnum contribute most greatly toward the high covariation coefficient. The high covariance between these bones implies a tightly associated morphological relationship between trapezoid and magnum. In the larger *T. indicus*, the less concave margins and relatively greater articular surface suggest greater immobility across this joint. In addition, we find that the scaphoid facet for the trapezoid is more concave, thus allowing less mobility for the trapezoid within the *T. indicus* carpus; this finding should be treated with some caution, as this feature was not revealed to be statistically significant after covariation analysis ($p = .08$). Despite the poor co-variation between the trapezoid and scaphoid, evidence from the trapezoid-magnum facet implies the morphology of *T. indicus* is adapted for greater loading on the medial digit than other modern tapirs, allowing greater force transmission through the medial carpus. This conclusion is further supported by results for metacarpal morphology in this study (see below) and conclusions from previous qualitative assessments (Earle, 1893; Gregory, 1929). When combined with other subtle differences in the carpal complex of *T. indicus*, the adaptation of the trapezoid-magnum joint suggests the medial manus of *T. indicus* may be loaded more heavily relative to other tapirs,

despite maintaining anatomical mesaxonic symmetry. By contrast, *T. bairdii* displays the least concave trapezoid facet on the scaphoid, with both *T. terrestris* and *T. pinchaque* displaying very similar trapezoid-magnum (Figure 9c,d) and trapezoid-scaphoid facet morphologies, intermediate between *T. indicus* and *T. bairdii*. This similarity may signify a phylogenetic aspect to this morphological difference (Ruiz-García et al., 2012, 2016). Further investigation into the carpal morphology of closely related South American taxa (e.g., the extinct *T. cristatellus* and *T. rondoniensis*) may shed more light on the evolutionary history of this morphology.

4.4 | Metacarpophalangeal facet variation

The tapir metacarpals display anatomical mesaxonic symmetry (axis of symmetry passing through the third digit), both in absolute length and in average centroid size (Table 2). Whereas the central third metacarpal exhibits discriminant variation in the proximal joint surfaces, the second, fourth, and fifth metacarpals are most successfully discriminated interspecifically using landmarks describing the palmar metacarpopalangeal joint (Figure 10). The metacarpophalangeal joint includes three main regions (the medial sesamoid facet, lateral sesamoid facet, and metacarpal sagittal ridge), all of which are described in part by the landmark analysis. The palmar section of the metacarpophalangeal joint facet articulates with the proximal phalange in addition to the paired sesamoid bones, which slot either side of the sagittal ridge (Constantinescu et al., 2012; Liebich et al., 2007). Quantitative comparisons of this facet across the four metacarpals demonstrated that the facet morphology of each type of metacarpal is significantly different, as are the differences between species ($p < .001$; Table 3). Two taxa stand out as notably different in their palmar metacarpophalangeal joint morphology: *T. indicus* and *T. pinchaque*.

T. indicus demonstrates a suite of adaptations for increased forelimb loading, as has been shown in previous literature and in this study (Earle, 1893; Gregory, 1929; Hulbert, 1995; MacLaren & Nauwelaerts, 2016). The palmar facet of the metacarpals also shows adaptations for increased bone-bone contact, with *T. indicus* demonstrating a relatively broad facet on all metacarpals (Figure 10), in addition to adaptations to the medial and lateral carpus enabling dissipation of compressive forces (Figure 9). Furthermore, the sagittal ridge of the metacarpals in *T. indicus* is elongated proximally, with mediolaterally broad sesamoid facets, offering large sesamoids a greater surface area with which to articulate. We interpret this as an adaptation contributing to load distribution across each metacarpal, and by extension the entire foot (Easton & Kawcak, 2007). Interestingly, this morphology of the palmar sagittal ridge is mirrored in *T. pinchaque*, which is on average the smallest and least massive of the neotropical taxa. As it is unlikely that *T. pinchaque* would require increased sesamoid-metacarpal contact to overcome high loading due to increased mass (i.e., graviportalism), we hypothesise that this shift in morphology in *T. pinchaque* is consistent with conferring greater stability to each toe (Hildebrand, 1985) and spreading the forces more evenly during limb loading (Easton & Kawcak, 2007). We also infer that, as this feature is seen in all the metacarpals of *T. pinchaque*, that the distal forelimb of this species has developed increased stability in all its digits. Impact of the fifth digit on the substrate would greatly benefit the animal, especially under potentially high loading conditions such as running up a steep, forested incline. Increased loading and necessity for stability in this comparatively small tapir may be due to a number of factors. Reduced reliance on the digital pad in favour of the toes, as is seen through equid evolution (MacFadden, 1992; Thomason, 1985), would cause a shift in loading forces to the toes and may account for increased sesamoid facets and necessity for toe stability in *T. pinchaque*. No quantitative comparisons of toepad size has been reported in *T. pinchaque*, and so this interpretation remains speculative until further investigation has been undertaken. In addition, moving up or down sub-alpine habitats and over uneven, high altitude wet-grassland (Downer, 1996; Padilla et al., 2010) would necessitate increased digital stability; this supports previous quantitative results on forelimb morphology and biomechanics in this species (MacLaren & Nauwelaerts, 2016). We find further support for previous quantitative works (Hawkins, 2011; MacLaren & Nauwelaerts, 2016) in the overall shape of *T. pinchaque* metacarpals, which demonstrate a more gracile morphology than those of other extant taxa. Overall, the adaptations observed in *T. pinchaque* in this and other osteological studies hint at the retention or re-exploration of putatively 'primitive' perissodactyl forelimb traits (e.g., equal force distribution from lunate to unciform and magnum; functional fifth digit; gracile long bones), while concurrently developing novel adaptations to both the upper and lower forelimb (e.g., large supraspinous fossa as potential proximal shock absorber; braced resting stance; strongly keeled metacarpophalangeal joints increasing stability for the phalanges during locomotion) (this study; MacLaren & Nauwelaerts, 2016).

Finally, when compared to the metacarpals of other extant taxa, *T. bairdii* demonstrates the least proximal enlargement of the palmar sagittal ridges, more notably on MC2 and MC4 (Figure 10). *T. bairdii* also demonstrates a compressed proximal carpal row, indicative of resistance to compressive forces in large quadrupeds (Prothero, 2005), which may represent an adaptation toward graviportalism not seen in the upper forelimb of this species. The manus of *T. bairdii* demonstrates greater potential for mobility of the medial digit (MC2; Figure 9), and small centroid size of MC5 compared to that of other neotropical species (Table 2). From these adaptations, we posit that *T. bairdii*, despite its large size, has reduced functionality of the most lateral digit in favour of the second, third and fourth digits, strongly supporting both anatomical and biomechanical mesaxonic symmetry in this taxon. In contrast, the anatomical features of the autopodium in *T. indicus* demonstrate adaptations for broader force dissipation across the four digits of the manus; as such, *T. indicus* is the only extant tapir that may not adhere to both anatomical and biomechanical interpretations of mesaxonic symmetry. Kinematic and kinetic research will be necessary to shed greater light upon actual limb loading regimes in this enigmatic, and variable, group of mammals.

5 | CONCLUSIONS

From both qualitative and quantitative comparisons of the tapir fore-foot, we formulated several hypotheses regarding the

morphology of modern tapir carpals and metacarpals, investigating whether the anatomy of the tapir autopodium supports both anatomical and biomechanical interpretations of mesaxonic symmetry. Discriminant function results support our hypothesis that *T. indicus* is morphologically separate from neotropical tapirs, although conclusions from previous studies regarding carpal morphology and function are shown to require rigorous reassessment. Interspecific differences among neotropical taxa do not align with previous quantitative comparisons of the forelimb (MacLaren & Nauwelaerts, 2016), with *T. bairdii* rather than *T. pinchaque* displaying the most divergent neotropical morphologies. Interspecific comparisons and covariance analyses of the autopodials offer evidence that *T. indicus* has adapted its metapodials and distal carpals to cope with higher loading forces than other tapirs, which supports all previous assessments on tapir limb morphology. Morphometric analysis suggests that *T. bairdii* places greater reliance on digits II, III, and IV than other species, with a decreased load predicted for digit V due to size and distal joint morphology. Testing this will require further analysis of the kinematics of locomotion in living tapirs. Conversely, *T. indicus* and *T. pinchaque* demonstrate osteological evidence for functional use of the fifth digit, widely considered as redundant in neotropical tapirs (Earle, 1893; Osborn, 1929). These and other features of the autopodium lead us to believe that both *T. indicus* and *T. pinchaque* have retained a fully functional tetradactyl manus, and *Tapirus* as a genus may not necessarily display both anatomical and biomechanical mesaxonic symmetry as has previously been supposed. We conclude that the tetradactyl tapir manus should be considered as a variable locomotor unit with a spectrum of functional adaptations, rather than simply a lingering plesiomorphy.

ACKNOWLEDGMENTS

The authors would like to thank Chris Conroy (MVZ), Christiane Funk (ZMB), Eleanor Hoeger (AMNH), Pepijn Kamminga (RMNH), Josephine Lesur (MNHN), Luc Tyteca (MEO), and Frank Zachos (NHMW) for provision of museum specimens for this study. The authors would also like to thank two anonymous reviewers who provided excellent feedback and ideas for improving the study. Finally, we would like to thanks Peter Aerts for assistance in finalising the revised manuscript. This study was financially supported by a FWO (Fonds Wetenschappelijk Onderzoek) scholarship awarded to JM and BOF-UA (Special Research Fund for Universiteit Antwerpen) research grant awarded to SN.

REFERENCES

Adams, D. C., Rohlf, F. J., & Slice, D. E. (2004). Geometric morphometrics: Ten years of progress following the "revolution. *Italian Journal of Zoology*, *71*(1), 5–16.

Bressou, C. (1961). La myologie du tapir (*Tapirus indicus* L.). *Mammalia*, *25*(3), 358–400.

Brown, J. C., & Yalden, D. W. (1973). The description of mammals – 2 Limbs and locomotion of terrestrial mammals. *Mammal Review*, *3*(4), 107–134.

Budras, K.-D., Sack, W. O., & Rock, S. (2003). Thoracic limb. In K.-D. Budras, W. O. Sack, & S. Rock (Eds.), *Anatomy of the horse* (pp. 2–13). Stuttgart: Schlutersche.

Campbell, B. (1936). The comparative myology of the forelimb of the hippopotamus, pig and tapir. *Americal Journal of Anatomy*, *59*(2), 201–247.

Cignoni, P., Callieri, M., Corsini, M., Dellapiane, M., Ganovelli, F., & Ranzuglia, G. (2008). MeshLab: an open-source mesh processing tool. In V. Scarano, R. De Chiara, & U. Erra (Eds.), *Eurographics Italian Chapter Conference* (pp. 1–8). Salerno.

Clayton, H. M., Chateau, H., & Back, W. (2013). Forelimb function. In W. Back & H. M. Clayton (Eds.), *Equine locomotion* (pp. 99–125). London: Saunders Elsevier.

Colbert, M. W. (2005). The facial skeleton of the early Oligocene *Colodon* (Perissodactyla, Tapiroidea). *Palaeontologia Electronica*, *8*(1), 1–27.

Constantinescu, G. M., Habel, R. E., Hillebrand, A., Sack, W. O., Schaller, O., Simoens, P., & de Vos, N. R. (2012). *Illustrated Veterinary Anatomical Nomenclature Third*. In G. M. Constantinescu & O. Schaller (Eds.), (pp. 10–62) Stuttgart: Enke.

Cozzuol, M. A., Clozato, C. L., Holanda, E. C., Rodrigues, F. H. G., Nienow, S., de Thoisy, B., Redondo, R. A. F., & Santos, F. R. (2013). A new species of tapir from the Amazon. *Journal of Mammalogy*, *94*(6), 1331–1345.

Downer, C. C. (1996). The mountain tapir, endangered "flagship" species of the high Andes. *Oryx*, *30*(1), 45–58.

Earle, C. (1893). Some points in the comparative osteology of the tapir. *Science 21*(526), 118.

Earle, C. (1896). Tapirs past and present. *American Journal of Science*, *4* (104), 934–935.

Easton, K. L., & Kawcak, C. E. (2007). Evaluation of increased subchondral bone density in areas of contact in the metacarpophalangeal joint during joint loading in horses. *American Journal of Veterinary Research*, *68*(8), 816–821.

Fadda, C., & Corti, M. (2001). Three-dimensional geometric morphometrics of *Arvicanthis*: Implications for systematics and taxonomy. *Journal of Zoological Systematics and Evolutionary Research*, *39*(4), 235–245.

Gould, F. D. H. (2014). To 3D or not to 3D, that is the question: Do 3D surface analyses improve the ecomorphological power of the distal femur in placental mammals? *PLoS One*, *9*(3), e91719.

Gregory, W. K. (1929). Mechanics of locomotion in the evolution of limb structure as bearing on the form and habits of the titanotheres and the related odd-toed ungulates. In H. F. Osborn (Ed.), *The titanotheres of ancient Wyoming, Dakota and Nebraska* (pp. 727–756). Washington, DC: United States Government Printing Office.

Hawkins, P. L. (2011). *Variation in the modified first metatarsal of a large sample of Tapirus polkensis, and the functional implication for Ceratomorphs*. East Tennessee State University.

Hellmund, M. (2005). *A three-dimensional skeletal reconstruction of the Middle Eocene Propalaeotherium hassiacum Haupt 1925 (Equidae, Perissodactyla, Mammalia) and a modern synoptic painting of some individuals within their habitat*. Current Research in Vertebrate Palaeontolgy 3rd Annual Meeting of the European Association of Vertebrate Palaeontologists (EAVP; p. 15). Hessisches Landesmuseum Darmstadt.

Hershkovitz, P. (1954). Mammals of Northern Colombia, Preliminary Report No. 7: Tapirs (genus *Tapirus*) with a systematic review of American species. *Proceedings of the United States National Museum*, *103*, 465–496.

Hildebrand, M. (1985). Walking and running. In M. Hildebrand, et al., (Eds.), *Functional vertebrate morphology* , (pp. 38–57). Cambridge: Harvard University Press

Holanda, E. C., Ribeiro, A. M., & Ferigolo, J. (2012). New material of *Tapirus* (Perissodactyla: Tapiridae) from the Pleistocene of southern Brazil. *Revista Mexicana De Ciencias Geologicas*, *29*(2), 308–318.

Holbrook, L. (2001). Comparative osteology of early Tertiary tapiromorphs (Mammalia, Perissodactyla). *Zoological Journal of the Linnean Society*, *132*(1), 1–54.

Holbrook, L. T. (1999). The phylogeny and classification of tapiromorph perissodactyls (Mammalia). *Cladistics*, *15*(3), 331–350.

Holbrook, L. T. (2009). Osteology of *Lophiodon* Cuvier, 1822 (Mammalia, Perissodactyla) and its phylogenetic implications. *Journal of Vertebrate Paleontology*, *29*(1), 212–230.

Hulbert, R. C. (1995). The giant tapir, *Tapirus haysii*, from Leisey Shell Pit 1A and other Florida Irvingtonian localities. *Bulletin of the Florida Museum of Natural History*, *37*(16), 515–551.

Hulbert, R. C. (2005). Late Miocene *Tapirus* (Mammalia, Perissodactyla) from Florida, with description of a new species, *Tapirus webbi*. *Bulletin of the Florida Museum of Natural History*, *45*(4), 465–494.

Hulbert, R. C. (2010). A new early Pleistocene tapir (Mammalia: Perissodactyla) from Florida, with a review of Blancan tapirs from the state. *Bulletin of the Florida Museum of Natural History*, *49*(3), 67–126.

Hulbert, R. C., Wallace, S. C., Klippel, W. E., & Parmalee, P. W. (2009). Cranial morphology and systematics of an extraordinary sample of the Late Neogene dwarf tapir, *Tapirus polkensis* (Olsen). *Journal of Paleontology*, *83*(2), 238–262.

IBM Corp. (2013). IBM SPSS Statistics for Windows, Version 22.0. Armonk, NY: IBM Corp.

Janis, C. (1984). Tapirs as living fossils. In N. Eldredge & S. M. Stanley (Eds.), *Living fossils. Casebooks in earth sciences* (pp. 80–86). New York, NY: Springer New York.

Janis, C. M. (1989). A climatic explanation for patterns of evolutionary diversity in ungulate mammals. *Palaeontology*, *32*(3), 463–481.

Klaits, B. G. (1972). The moving mesaxonic manus—A comparison of tapirs and rhinoceroses. *Mammalia*, *36*(1), 126–145.

Klingenberg, C. P. (2009). Morphometric integration and modularity in configurations of landmarks: Tools for evaluating a priori hypotheses. *Evolution & Development*, *11*(4), 405–421.

Klingenberg, C. P. (2011). MorphoJ: An integrated software package for geometric morphometrics. *Molecular Ecology Resources*, *11*(2), 353–357.

Liebich, H.-G., Konig, H. E., & Maierl, J. (2007). Forelimb or thoracic limb (membra thoracica). In H. E. Konig & H.-G. Liebich (Eds.), *Veterinary anatomy of domestic animals: Textbook and colour atlas* (pp. 145–214). Stuttgart: Schlutersche.

Lockley, M. G. (2009). New perspectives on morphological variation in tridactyl foot prints : Clues to widespread convergence in developmental dynamics. *Geological Quarterly*, *53*(4), 415–432.

MacFadden, B. J. (1992). *Fossil horses: Systematics, paleobiology and evolution of the family equidae*. Cambridge: Cambridge University Press.

MacLaren, J. A., & Nauwelaerts, S. (2016). A three-dimensional morphometric analysis of upper forelimb morphology in the enigmatic tapir (Perissodactyla: *Tapirus*) hints at subtle variations in locomotor ecology. *Journal of Morphology*, *277*(11), 1469–1485.

Murie, J. (1871). The Malayan tapir. *Journal of Anatomy and Physiology*, *6* (1), 131–512.

Nauwelaerts, S., Vangeel, K., & Aerts, P. (2016). *Loading distribution over the four fingers of the tapir during locomotion*. 11th International Congress of Vertebrate Morphology, Washington, DC.

Norman, J. E., & Ashley, M. V. (2000). Phylogenetics of Perissodactyla and tests of the molecular clock. *Journal of Molecular Evolution*, *50*(1), 11–21.

Osborn, H. F. (1929). Theories as to the origin, ancestry, and adaptive radiation of the titanotheres and other odd-toed ungulates. In H. F. Osborn (Ed.), *The titanotheres of ancient Wyoming, Dakota and Nebraska* (pp. 757–804). Washington, DC: United States Government Printing Office.

Padilla, M., Dowler, R. C., & Downer, C. C. (2010). *Tapirus pinchaque* (Perissodactyla: Tapiridae). *Mammalian Species*, *42*(1), 166–182.

Pereira, S. G. (2013). *Anatomia ossea, muscular e consideracoes adaptativas do membro toracico de Tapirus terrestris (Perissodactyla, Tapiridae)*. (pp. 1–76). Universidade Federal de Uberlandia (thesis). Minas Gerais, Brazil.

Prothero, D. R. (2005). Postcranial osteology. In *The evolution of North American Rhinoceroses* (pp. 146–181). Cambridge: Cambridge University Press.

R Core Development Team. (2008). *R: A language and environment for statistical computing*. R Foundation for Statistical Computing, Vienna, Austria.

Radinsky, L. B. (1965). Evolution of the tapiroid skeleton from *Heptodon* to *Tapirus*. *Bulletin of the Museum of Comparative Zoology*, *134*, 69–106.

Rajkumar, H. S., & Klein, H. (2014). First perissodactyl footprints from Flysch deposits of the Barail Group (Lower Oligocene) of Manipur, India. *Proceedings of the Indian Academy of Sciences. Earth and Planetary Sciences*, *123*(2), 413–420.

Reghem, E., Byron, C., Bels, V., & Pouydebat, E. (2012). Hand posture in the grey mouse lemur during arboreal locomotion on narrow branches. *Journal of Zoology*, *288*(1), 76–81.

Rohlf, F. J., & Corti, M. (2000). Use of two-block partial least-squares to study covariation in shape. *Systematic Biology*, *49*(4), 740–753.

Rohlf, F. J., & Slice, D. (1990). Extensions of the Procrustes method for the optimal superimposition of landmarks. *Systematic Zoology*, *39*(1), 40–59.

Ruiz-García, M., Vásquez, C., Pinedo-Castro, M., Sandoval, S., Castellanos, A., Kaston, F., de Thoisy, B., Shostell, J. (2012). Phylogeography of the mountain tapir (*Tapirus pinchaque*) and the Central American tapir (*Tapirus bairdii*) and the origins of the three Latin-American tapirs by means of mtCyt-B sequences. In K. Anamthawat-Jnsson (Ed.), *Current topics in phylogenetics and phylogeography of terrestrial and aquatic systems* (pp. 83–116). InTech. Retrieved from https://www.intechopen.com/books/

Ruiz-García, M., Castellanos, A., Bernal, L. A., Pinedo-Castro, M., Kaston, F., & Shostell, J. M. (2016). Mitogenomics of the mountain tapir (*Tapirus pinchaque*, Tapiridae, Perissodactyla, Mammalia) in Colombia and Ecuador: Phylogeography and insights into the origin and systematics of the South American tapirs. *Mammalian Biology - Zeitschrift Für Säugetierkunde*, *81*(2), 163–175.

Schoch, R. M. (1989). A review of the tapiroids. In D. R. Prothero & R. M. Schoch (Eds.), *The evolution of perissodactyls* (pp. 299–320). New York: Oxford University Press.

Simpson, G. G. (1945). Notes on Pleistocene and recent tapirs. *Bulletin of the American Museum of Natural History*, *86*(2), 33–82.

Steiner, C. C., & Ryder, O. A. (2011). Molecular phylogeny and evolution of the Perissodactyla. *Zoological Journal of the Linnean Society*, *163*(4), 1289–1303.

de Thoisy, B., Pukazhenthi, B., Janssen, D. L., Torres, I. L., May Jr., J. A., Medici, P. . . . Quse, V. (2014). *Tapir Veterinary Manual* (2nd ed.). In V. Quse & R. C. Fernandes-Santos (Eds.), IUCN/SSC Tapir Specialist Group.

Thomason, J. J. (1985). Estimation of locomotory forces and stresses in the limb bones of recent and extinct equids. *Paleobiology*, *11*(2), 209–220.

Tougard, C., Delefosse, T., Hänni, C., & Montgelard, C. (2001). Phylogenetic relationships of the five extant Rhinoceros species

(Rhinocerotidae, Perissodactyla) based on mitochondrial cytochrome b and 12S rRNA genes. *Molecular Phylogenetics and Evolution*, *19*(1), 34–44.

Wiley, D. F., Amenta, N., Alcantara, D. A., Ghosh, D., Kil, Y. J., Delson, E., … O'Neill, R. (2005). Evolutionary morphing. In: IEEE Visualization. VIS 05. Minneapolis, MN, USA. 431–438.

Wood, A. R. et al. (2010). Postcranial functional morphology of *Hyracotherium* (Equidae, Perissodactyla) and locomotion in the earliest horses. *Journal of Mammalian Evolution*, *18*(1), 1–32.

Yalden, D. W. (1971). The functional morphology of the carpus in ungulate mammals. *Cells Tissues Organs*, *78*(4), 461–487.

Zelditch, M. L., Swiderski, D. L., & Sheets, H. D. (2012). *Geometric morphometrics for biologists: A primer*. New York: Academic Press.

SUPPORTING INFORMATION

Additional Supporting Information may be found online in the supporting information tab for this article.

How to cite this article: MacLaren JA, Nauwelaerts S. Interspecific variation in the tetradactyl manus of modern tapirs (Perissodactyla: *Tapirus*) exposed using geometric morphometrics. *Journal of Morphology*. 2017;00:1–19. https://doi.org/10.1002/jmor.20728

SGML and CITI Use Only
DO NOT PRINT

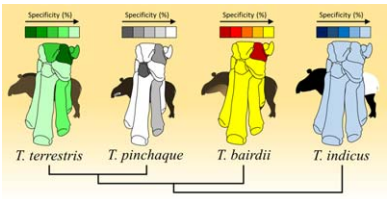

A simplified phylogeny demonstrating gross differences in the manus morphology of modern tapirs. Bones with lighter colours (higher specificity %) represent higher levels of morphological difference between species, darker colours represent bones that are misclassified more frequently. Each tapir species is represented by a silhouette diagram demonstrating generalised appearance.